HHS Public Access

Author manuscript

J Immunol. Author manuscript; available in PMC 2021 February 01.

Published in final edited form as:

J Immunol. 2020 February 01; 204(3): 644–659. doi:10.4049/jimmunol.1901211.

IL-10 impairs local immune response in lung granulomas and lymph nodes during early *Mycobacterium tuberculosis* infection

Eileen A. Wong[1], **Stephanie Evans**[2], **Carolyn R. Kraus**[3], **Kathleen D. Engelman**[3], **Pauline Maiello**[1], **Walter J. Flores**[3], **Anthony M. Cadena**[1], **Edwin Klein**[4], **Kayla Thomas**[1], **Alexander G. White**[1], **Chelsea Causgrove**[1], **Brianne Stein**[1], **Jaime Tomko**[1], **Joshua T. Mattila**[5], **Hannah Gideon**[1], **P. Ling Lin**[6], **Keith A. Reimann**[3], **Denise E. Kirschner**[2], **JoAnne L. Flynn**[1]

[1]Department of Microbiology and Molecular Genetics, University of Pittsburgh School of Medicine, Pittsburgh PA

[2]Department of Microbiology and Immunology, University of Michigan Medical School, Ann Arbor, MI

[3]Non-human Primate Reagents Resources, MassBiologics, University of Massachusetts Medical School, Boston MA

[4]Division of Laboratory Animal Resources, University of Pittsburgh, Pittsburgh PA

[5]Department of Infectious Diseases and Microbiology, University of Pittsburgh School of Public Health, Pittsburgh PA

[6]Department of Pediatrics, UPMC Children's Hospital of Pittsburgh, University of Pittsburgh School of Medicine

Abstract

Tuberculosis (TB), caused by *Mycobacterium tuberculosis* (Mtb), continues to be a major global health problem. Lung granulomas are organized structures of host immune cells that function to contain the bacteria. Cytokine expression is a critical component of the protective immune response but inappropriate cytokine expression can exacerbate TB. While the importance of pro-inflammatory cytokines in controlling Mtb infection has been established, the effects of anti-inflammatory cytokines, such as IL-10, in TB are less well understood. To investigate the role of IL-10, we used an antibody to neutralize IL-10 in cynomolgus macaques during Mtb infection. Anti-IL-10 treated NHPs had similar overall disease outcomes compared to untreated control NHPs, but there were immunological changes in granulomas and lymph nodes from anti-IL-10 treated animals. There was less thoracic inflammation and increased cytokine production in lung granulomas and lymph nodes from IL-10 neutralized animals at 3-4 weeks post-infection compared to control animals. At 8 weeks post-infection, lung granulomas from IL-10 neutralized animals had reduced cytokine production but increased fibrosis relative to control animals. While these immunological changes did not affect the overall disease burden during the first 8 weeks of infection, we paired computational modeling to explore late infection dynamics. Our findings support that early changes occurring in the absence of IL-10 may lead to better bacterial control

Corresponding Author: JoAnne L. Flynn, phone: 412-624-7743, fax: 412-648-9076; joanne@pitt.edu.

later during infection. These unique datasets provide insight into the contribution of IL-10 to the immunological balance necessary for granulomas to control bacterial burden and disease pathology in Mtb infection.

Introduction

Tuberculosis (TB) continues to be a major cause of death worldwide, with 1.6 million deaths from TB in 2017 alone (1). Despite decades of research, the nuances of the complex relationship between the host response and *Mycobacterium tuberculosis (*Mtb) remain unclear. In the best-case scenario, host immune cells coordinate their responses to contain the bacteria, in a delicate balance of killing Mtb or halting bacterial spread without causing excessive disease pathology. After Mtb bacilli are inhaled, they are phagocytosed by alveolar macrophages, and a subsequent influx of other innate immune cells, such as neutrophils and dendritic cells, are recruited to the site of infection in the lung parenchyma to assist in containing Mtb (2-5). Once adaptive immune responses are initiated in the lung draining lymph nodes, T cells and B cells traffic to the site of infection to assist innate immune responses (6-10). Together, these host immune cells form an organized structure of a granuloma that acts to kill or contain the bacteria, preventing further bacterial spread. Both innate and adaptive immune cells and their cytokine responses have been established to be critical for control and clearance of Mtb (reviewed in (11-14)). However, not all granulomas are successful at killing or containing the infection, and there is extensive variability among immune responses and infection outcome at the granuloma level, even in a single host (15).

The host immune responses early in infection are critical for eventual disease outcome. Humans infected with Mtb have clinical signs of early initial inflammatory responses (initial fevers and elevated erythrocyte sedimentation rates) and lymph node involvement (hilar adenopathy) usually within the first two months of infection (16, 17). Studies in non-human primates (NHPs) and computational modeling also support the importance of these early immune events on eventual disease outcome, with robust bacterial killing in granulomas only after about 10 weeks of infection (18-20). Many host immune cells and their cytokine responses have been to be important for control of Mtb infection. In particular, pro-inflammatory cytokines produced by T cells, such as IFN-γ, TNF, and IL-17, have been shown in humans, NHPs, and mice to be critical for optimal control of Mtb (13, 14, 21-32). However, uncontrolled inflammatory cytokine responses from these immune cells can also cause damage to tissues, leading to increased inflammation and exacerbation of TB disease.

The immune response has many checks and balances to counter a pro-inflammatory response and prevent damage. One major factor that can prevent tissue damage is IL-10, a cytokine with anti-inflammatory properties (33). IL-10 can be produced by many immune cells, including monocytes, macrophages, dendritic cells, B cells, NK cells, mast cells, and nearly all T cell subsets (34). Dysregulation of IL-10 has been associated with negative disease outcomes in bacterial and viral infections and autoimmune or inflammatory diseases (33, 35, 36).

Several studies have investigated the role of IL-10 in Mtb infections, but the cumulative results are inconclusive. Elevated levels of IL-10 in patients have been suggested to be

associated with more active or severe cases of TB (37-39), and blocking IL-10 improved Th1 and macrophage function in *in vitro* studies (40, 41). Mice impaired for IL-10 expression or function have improved bacterial control and enhanced survival during Mtb infections (42-46), while overexpressing IL-10 increased bacterial burden and exacerbation of the disease (47-49). In contrast, other studies in mice indicated that lack of IL-10 had insignificant effects on the bacterial burden during Mtb infections, but resulted in detrimental immunopathology and decreased survival in some studies (50-53). While many of these studies indicate that IL-10 during Mtb infection may be restricting Th1 function and preventing a sufficient immune response that reduces bacterial burden, some of these studies also implicate IL-10 in preventing or reducing immunopathology. These differences may depend on the relative susceptibility and intensity of IL-10 response to Mtb infection in the mouse strains used in these studies. Further contributing to these contradictory results, some studies suggest that IL-10 may have differential effects depending on the stage of Mtb infection. Blocking IL-10 later in infection (after 3 months) partially reduced bacterial burden (42), but transiently blocking IL-10 during the first month of infection had even greater effects on the long-term control of Mtb infection (43). Most of these studies were based on whole organ or whole animal outcomes and there are few studies of individual TB granulomas. Computational modeling of TB granulomas indicated that IL-10 within the granulomas was necessary to reduce excessive inflammation (20). In granulomas from Mtb-infected macaques, T cells expressing IL-10 in conjunction with T cells expressing pro-inflammatory cytokines, such as IL-17, were associated with improved sterilization of Mtb (15).

To address the role of IL-10 in an animal model that recapitulates all aspects of human Mtb infection, including pathology, we used a macaque-specific anti-IL-10 neutralizing antibody to manipulate the levels of active IL-10 *in vivo* during Mtb infection of cynomolgus macaques. This provided the opportunity to address the role of IL-10 at critical, early time points after infection, as the immune cells establish in the lungs and form granulomas. We found that IL-10 neutralization reduced early inflammation, as assessed by PET CT imaging, in a subset of granulomas, which resulted in lower bacterial burden in that granuloma subset. However, total thoracic bacterial burden was not significantly different between IL-10 neutralized and control animals. IL-10 neutralization also resulted in increased levels of some cytokines in lung granulomas and thoracic lymph nodes at 4 weeks of Mtb infection. However, by 8 weeks post-infection, the cytokine responses in lung granulomas and lymph nodes decreased or stabilized. IL-10 neutralization also increased collagenization and fibrosis in lung granulomas by 8 weeks post-infection. Using computational modeling of TB granulomas to extend the time frame of our study, we determined that these early cytokine changes and increased collagenization may lead to improved bacterial control during long-term Mtb infection. Thus, IL-10 neutralization influenced the cytokine response in lung granulomas and lymph nodes early in Mtb infection, but did not affect overall bacterial burden or disease. However, reduced IL-10 may set the stage for better bacterial control over a longer infection period.

Materials and Methods

Animal Ethics Statement

All experimental manipulations, protocols, and care of the animals were approved by the University of Pittsburgh School of Medicine Institutional Animal Care and Use Committee (IACUC). The DLAR and IACUC adheres to national guidelines established in the Animal Welfare Act (7 U.S.C. Sections 2131–2159) and the Guide for the Care and Use of Laboratory Animals (8th Edition) as mandated by the U.S. Public Health Service Policy. All macaques used in this study were housed at the University of Pittsburgh in rooms with autonomously controlled temperature, humidity, and lighting. Animals were singly housed in caging at least 2 square meters apart that allowed visual and tactile contact with neighboring conspecifics. The macaques were fed twice daily with biscuits formulated for nonhuman primates, supplemented at least 4 days/week with large pieces of fresh fruits or vegetables. Animals had access to water ad libitem. Because our macaques were singly housed due to the infectious nature of these studies, an enhanced enrichment plan was designed and overseen by our nonhuman primate enrichment specialist. This plan has three components. First, species-specific behaviors are encouraged. All animals have access to toys and other manipulata, some of which will be filled with food treats (e.g. frozen fruit, peanut butter, etc.). These are rotated on a regular basis. Puzzle feeders foraging boards, and cardboard tubes containing small food items also are placed in the cage to stimulate foraging behaviors. Adjustable mirrors accessible to the animals stimulate interaction between animals. Second, routine interaction between humans and macaques are encouraged. These interactions occur daily and consist mainly of small food objects offered as enrichment and adhere to established safety protocols. Animal caretakers are encouraged to interact with the animals (by talking or with facial expressions) while performing tasks in the housing area. Routine procedures (e.g. feeding, cage cleaning, etc.) are done on a strict schedule to allow the animals to acclimate to a routine daily schedule. Third, all macaques are provided with a variety of visual and auditory stimulation. Housing areas contain either radios or TV/video equipment that play cartoons or other formats designed for children for at least 3 hours each day. The videos and radios are rotated between animal rooms so that the same enrichment is not played repetitively for the same group of animals. All animals are checked at least twice daily to assess appetite, attitude, activity level, hydration status, etc. Following Mtb infection, the animals are monitored closely for evidence of disease (e.g., anorexia, weight loss, tachypnea, dyspnea, coughing). Physical exams, including weights, are performed on a regular basis. Animals are sedated prior to all veterinary procedures (e.g. blood draws, etc.) using ketamine or other approved drugs. Regular PET-CT imaging is conducted on most of our macaques following infection and has proved very useful for monitoring disease progression. Our veterinary technicians monitor animals especially closely for any signs of pain or distress. If any are noted, appropriate supportive care (e.g. dietary supplementation, rehydration) and clinical treatments (analgesics) are given. Any animal considered to have advanced disease or intractable pain or distress from any cause is sedated with ketamine and then humanely euthanatized using sodium pentobarbital.

Macaque-specific anti-IL-10 antibody

The neutralizing anti-IL-10 antibody was constructed using the heavy and light chain variable regions of the humanized, anti-human IL-10 antibody, hu12G8 based on sequences from (54). This antibody showed similar affinity for human and macaque IL-10 (54). A macaque recombinant form of this antibody was expressed in Chinese hamster ovary cells as full-length Ig with rhesus IgG1 and kappa constant regions. A silencing mutation, L235A, L236A, was introduced into the rhesus heavy chain constant region to limit the antibody's effector function to cytokine neutralization.

The antibody was manufactured by shake flask production using stable-expressing CHO cells in chemically-defined, animal component-free medium and purified using protein A affinity chromatography. Cells were grown in 3 L shake flasks using proprietary media from Gibco. For each cell line the following specifications were followed; pH 7, 37°C, 110 RPM for agitation. The glucose concentration was monitored and maintained at a glucose concentration of 4.1 g/L. The glucose was monitored with NOVA bioanalyser 400 (Nova Biomedical, Deeside, UK). A proprietary feed was given every day starting on day 3 to day 14. On day 14, the flasks were harvested. Clarification: Depth Filters were used to clarify the 10 L cultured volume. The coarse filter used was Millistak® D0HC (0.6–9-μm nominal pore size) and size of 0.053 sq.m. The fine filter used was X0HC (<0.1-μm nominal pore size; EMD Millipore) and size of 0.054 sq.m. Depth filters were assembled in series and flushed with PBS pH 7.4. 10 L of culture was loaded through the filters and pressure was recorded. The pressure limit cut off was 25 PSI for the whole system in series. Finally, the clarified material was filtered with AcroPak 1500 Capsules with Supor Membrane-0.8/0.2um. Protein A Affinity Chromatography: Using an AKTA Pure 25 L, the anti-IL 10 antibody was purified. A 150 mL mAb Select™ packed column was used for the purification process. The column was equilibrated with binding buffer PBS pH 7.4. The clarified material was loaded through the column. The column was then washed with PBS pH 7.4 for 5 column volumes (750mL). Finally, the column was eluted with 20 mM Citrate, pH 3 for approximately 2 column volumes (300 mL). To neutralize the eluate 10 % of the total volume was used. The neutralization buffer was Trizma hydrochloride solution pH 8.0, 1M, BioReagent, Sigma Life Science added. Ultra Filtration and Diafiltration: Purified antibody was concentrated and buffer exchanged using Pellicon® XL50 with Biomax® 30 kDa Membrane, A screen, 50 cm^2. The product was concentrated up to 10 mg/mL and diafiltrated five times to a final formulation buffer of 20 mM Citrate, 150 mM NaCl pH 6.0. The concentration was measured using A280 spectrum with NanoDrop™ 2000/2000c Spectrophotometers. The extinction coefficient used at 280 nm for IL10 antibody was 1.44. Quality Control: Antibody was measured for percent monomer using Superdex 200 size exclusion column with UV detection at 280 nm. A >90 % monomer was verified and tested for endotoxin. The final purified material was tested for endotoxin using Endosafe PTS, Charles River. The final product passed the internal criteria of less than 5 EU/Kg, which is a level adopted from FDA guidelines. The final product was formulated in 20 mM sodium citrate buffer, pH 6.0, 150 mM sodium chloride, 0.02% Tween-80.

IL-10 neutralization in bioassays

D36 mouse mast cells (ATCC, Manassas, VA) were cultured in IMDM media (Sigma, St. Louis, MO) containing 10% FBS, 1% HEPES, 1mM sodium pyruvate, and 1% L-glutamine in the presence of 1ng/ml IL-3 and 1ng/ml IL-4. Cells were washed in PBS, counted by Trypan Blue exclusion, and resuspended in RPMI media (Sigma) containing 1% HEPES and 1% L-glutamine before resting for 3 hours at room temperature. Following rest, cells were counted again by Trypan Blue exclusion and aliquoted in sterile 96 well flat bottom plates at 100,000 cells/well in 100μl. Rhesus macaque IL-10 (kindly provided by Dr. Francois Villinger) was added to appropriate wells at a concentration of 20ng/ml. Macaque-IL-10-specific antibody (IL-10R1-LALA, MassBio, Cambridge, MA) was added to appropriate wells at varying concentrations (1–100 μg/ml). Samples were incubated for 18 hours at 37°C. Tritiated thymidine (PerkinElmer, Waltham, MA) was diluted in AIM V media (Gibco, Gaithersburg, MD) to a concentration of 20 μCi/ml and added to all samples before incubation for another 6 hours at 37°C. Cells were harvested onto glass fiber filters (PerkinElmer) before incorporated radioactivity was determined by liquid scintillation counting (TopCount, PerkinElmer).

IL-10 neutralization in *ex vivo* assays

Excised lung granulomas from cynomolgus macaques (*Macaca fascicularis*) designated for other studies were homogenized into a single cell suspension as previously described (55). Cell pellets were used for flow cytometry and supernatants were stored at −80°C until used for ELISAs. Cell pellets were resuspended in assay media (RPMI with 1% HEPES, 1% L-Glutamine, and 10% human AB serum) and equally divided into 2 wells in a sterile 96 well round bottom plate. Samples were washed with additional assay media. Sample halves designated for anti-IL-10 antibody neutralization treatment were resuspended in media containing anti-IL-10 antibody diluted in assay media for concentration of 10μg/ml (IL-10R1-LALA, MassBio, Cambridge, MA). Corresponding sample halves designated as media controls were resuspended in equal volumes of assay media. Samples were incubated overnight at 37°C. Following overnight incubation, samples were stimulated with peptide pools of Mtb-specific antigens ESAT-6 and CFP-10 (10μg/ml of each peptide) and Brefeldin A (GolgiPlug, BD Biosciences, San Jose, CA) for 3.5–4 hours at 37°C. Samples were then stained for viability (Invitrogen), cell surface markers, and intracellular cytokine markers. Cells were identified as T cells, with antibodies against CD3 (clone SP34–2), CD4 (clone L200), and CD8 (clone SK1). Following permeabilization using Fixation/Permeabilization solution (BD Biosciences), cytokine and cellular response were identified using antibodies against IFN-γ (clone B27), IL-2 (clone MQ1–17H12), TNF (clone MAB11), IL-17 (clone eBio64CAP17), IL-10 (clone JES3–9D7), and Ki67 (clone B56). Data acquisition was performed using a LSRII (BD) and analyzed using FlowJo Software v.9.7 (Treestar Inc, Ashland, OR).

Stored supernatants were thawed and filtered using 0.22μm syringe filter into ~1ml aliquots immediately before assay to prevent freeze-thaw cycles. Concentrations of IL-10 were detected using a NHP-specific IL-10 enzyme-linked immunosorbent assay (ELISA) (U-Cytech, Utrecht, The Netherlands) according to manufacturer's directions. Samples were

measured at OD450 on a spectrophotometer (SpectraMax, Molecular Devices, San Jose, CA).

Experimental animals, anti-IL-10 antibody infusions, and infections

Fourteen male cynomolgus macaques (*Macaca fascicularis*) between 5.7 and 8 years of age, with starting weights of 3.9–6.9 kg (Valley Biosystems, Sacramento, CA) were housed within Biosafety Level 3 (BSL-3) facilities as previously described (8, 28, 56) (IACUC protocol 16017309). Additional historical control samples from male animals from a previous study (57) (IACUC protocol 15066174) of similar age and weight infected with Mtb and necropsied at 4 weeks were also used in our analyses and differentiated as gray markers when included.

To assess the role of IL-10 in Mtb infections in our NHP model of Mtb infections, we designed an *in vivo* study using our anti-IL-10 neutralizing antibody. Macaques were sedated and given acetaminophen and diphenhydramine ≥ 30 minutes prior to infusion in both anti-IL-10 treatment and saline control groups. To neutralize IL-10 before the Mtb infection, macaques that were randomly designated for the anti-IL-10 treatment group were then infused with anti-IL-10 antibody (see above in Materials and Methods) diluted in saline at 15mg/kg over the course of 20–30 minutes, with pre-dosing, interim, and post-dosing vitals recorded, starting 1 day before Mtb infection. We chose a dose of 15mg/kg of anti-IL-10 antibody based on unpublished data from a similar human antibody in cynomolgus macaques, which indicated effectiveness without adverse side effects (David Sacks, personal communication). In two uninfected animals, infusion of 15 mg/kg or 30 mg/kg once resulted in anti-IL-10 antibody levels in serum at 15 days of 29 and 24 μg/ml respectively. Following the initial infusion prior to Mtb infection, to maintain IL-10 neutralization, macaques were infused with 15mg/kg of antibody every 10 days (+/−3 days) using the same procedure methods until necropsy, 4–8 weeks after initial infusion). Macaques randomly designated for the control group were sedated and treated the same as the anti-IL-10 treatment group, except infusions with 50ml of saline over 20–30 minutes. Three macaques were designated for the anti-IL-10 antibody treatment and 1 macaque was designated for the saline control group for the short 4 week study; 4 historical controls were included in the analysis. Five macaques were designated for the anti-IL-10 antibody treatment and 5 macaques were designated for the saline control group for the longer 8 week study.

Animals were infected with 9–19 colony forming units (CFU) of Mtb Erdman strain to the lower lung lobe by bronchoscopic instillation. Infection was confirmed and serial clinical, immunologic, and radiographic examinations were conducted during the course of the study as previously described (8, 18, 19, 55, 58, 59). Specifically, blood was serially drawn immediately prior to infusions, and TB granuloma formation and progression were tracked by serial ^{18}F-FDG PET-CT imaging, and their relative metabolic activity (FDG activity) as a proxy for inflammation measured as ^{18}F-FDG standard uptake values normalized to muscle (SUV) (59).

Necropsy

After 4 or 8 weeks of infection and infusions, necropsy of study animals was performed as previously described (8, 28, 55, 56, 60). In summary, 1–3 days prior to necropsy, individual granulomas were identified by ^{18}F-FDG PET-CT scans. At necropsy, NHPs were maximally bled and humanely sacrificed using pentobarbital and phenytoin (Beuthanasia, Schering-Plough, Kenilworth, NJ). During necropsy, gross disease pathology was quantified by a scoring system of number, size, and pattern of lung granulomas, and extent of disease involvement in lung lobes, mediastinal lymph nodes, and visceral organs, as previously described (8). Lymph nodes and PET-CT matched lung granulomas were excised for bacterial burden, immunological studies, and histological analyses. Representative sections of lymph nodes and lung granulomas were homogenized into single cell suspensions for bacterial quantification, flow cytometry, and multiplex immunoassays. Representative sections of lung granulomas were also formalin-fixed for immunohistochemistry and histology.

Bacterial quantification

Bacterial burden in individually excised granulomas, lymph nodes, representative lung lobe tissue, spleen, and liver were quantified by serial plating onto 7H11 medium and colony forming units (CFU) enumerated after 21 days of incubation at 37°C. Total thoracic CFU is calculated from summation of all lung, lung granuloma, and thoracic lymph node plated samples (61).

Flow cytometry of excised tissues

Single cell suspensions of homogenized tissues were incubated in the presence of Brefeldin A (GolgiPlug, BD Biosciences) for 2.5–3 hours at 37°C. Samples were washed with PBS, and stained for viability (Invitrogen), immune cell subsets, and intracellular cytokine markers. Cells were identified as T cells: CD3 (clone SP34–2), CD4 (clone L200), and CD8 (clone SK1); B cells: CD20 (clone 2H7); and macrophages and neutrophils: CD11b (clone ICRF44), CD163 (clone eBioGH1/61), calprotectin (clone 27E-10). Due to limitations in the panel, CD3+CD4− cells were used as an approximation for CD3+CD8+ T cells. Following permeabilization using FOXP3 staining kit (eBioscience), cytokine and cellular response were identified using antibodies against CD69 (clone TP1.55.3), IFN-γ (clone B27), IL-2 (clone MQ1-17H12), TNF (clone MAB11), IL-17 (clone eBio64CAP17), IL-10 (clone JES3–9D7), IL-6 (clone MQ2–6A3) and FOXP3 (clone PCH101). Data acquisition was performed using a LSRII (BD) and analyzed using FlowJo Software v.9.7 (Treestar Inc, Ashland, OR). Gating strategy is found in Supplemental Figure 1A.

Multiplex immunoassay

Total cytokine concentrations in lung granulomas and LNs were quantified using multiplex immunoassays. Supernatants from homogenized excised tissues stored at −80°C until time of assay. Supernatants were filtered using a 0.22μm syringe filter into ~1ml aliquots immediately before storage at −80°C or immediately before time of assay to minimize freeze-thaws. Cytokine and chemokine levels in thawed samples were measured by multiplex immunoassays specific for NHPs (ProcartaPlex, ThermoFisher Scientific,

Waltham, MA) according manufacturer's instructions. Immunoassay results were collected and analyzed using BioRad Bio-Plex 200 (BioRad, Hercules, CA).

Histopathology of tissues

A subset of tissues excised during necropsy, including lung granulomas and lymph nodes, were fixed in 10% neutral buffered formalin before placing in histology cassettes and paraffin-embedding. Sections of 5μm thick tissues were cut and mounted on SuperFrost Plus slides (ThermoFisher Scientific, Waltham, MA) and stained with hematoxylin and eosin by the University of Pittsburgh's in situ histology laboratory. Structural makeup of lung granulomas and extent of TB disease in LNs were examined and recorded by a veterinary pathologist who was blinded to treatment groups. Granulomas with histopathologic characteristics described with the terms "collagen", "fibrosis", or "fibroblasts" were scored as fibrotic.

Immunohistochemistry of paraffin-embedded granulomas

For collagen and fibrosis staining, a subset of granulomas was randomly selected for staining and analysis. Formalin-fixed paraffin-embedded tissue sections from animals included in this study were de-paraffinized and re-hydrated in sequential incubations in xylene, 95% ethanol, and 70% ethanol. Tissue sections were then incubated in a pressure cooker containing Tris-EDTA (pH 9) antigen retrieval buffer for 6 minutes under pressure. Samples were then depressurized and allowed to cool slowly over 30 minutes before washing in PBS. Samples were incubated in blocking buffer (1%BSA in PBS) for 15–30 minutes in a dark humidified chamber before addition of primary antibody cocktails diluted in blocking buffer to sections for overnight incubation at 4°C in a dark humidified chamber. Primary antibodies that required biotinylated secondaries for detection were incubated in blocking buffer (1%BSA in PBS) for 15 minutes followed by incubation in an endogenous avidin-biotin blocking kit according to manufacturer's instructions (Abcam, Cambridge, MA).

Antibodies used in this study against CD3 (clone CD3–12, 1:200 dilution), collagen I (rabbit polyclonal, 1:100 dilution), SMAD3 (phosphoS423+S425) (clone EP823Y, 1:100 dilution), and STAT6 (phosphor Y641) (rabbit polyclonal, 1:50 dilution) were from Abcam (Cambridge, MA); CD11c (clone 5D11, 1:30 dilution) from Leica Microsystems (Buffalo Grove, IL); CD20 (clone L26, 1:100 dilution) from Agilent Dako (Santa Clara, CA); IL-10Rα (polyclonal, 1:150 dilution) from Millipore (Temecula, CA); vimentin (chicken polyclonal, 1:100 dilution) from Novus Biologicals (Centennial, CO); CD68 (clone KP1, 1:30 dilution), alpha-Smooth muscle actin (clone 1A4, 1:100 dilution), and CD163 (clone 10D6, 1:30 dilution) from ThermoFisher Scientific (Waltham, MA). After incubation with primary antibodies, sections were washed four times in PBS and incubated with secondary antibodies for 1 hour at room temperature in a dark humidified chamber. Secondary antibodies against primary host species were purchased from Jackson ImmunoResearch Laboratories (West Grove, PA) or ThermoFisher Scientific (Waltham, MA). Zenon label kits (ThermoFisher Scientific, Waltham, MA) were used according to manufacturer's instructions and biotinylated secondary antibodies were from BD Biosciences. Specificity of antibodies were confirmed using no-primary controls using the same staining and imaging

protocol on serial sections. After secondary antibody incubation, slides were washed four times in PBS and mounted using ProLong Gold mounting medium with DAPI (Life Technologies, Eugene, OR). Slides were cured at room temperature for at least 24 hours and subsequently stored at −20°C. Slides were imaged using a Nikon immunofluorescent microscope with a scanning stage and saved as TIFF-format images.

Statistical analysis

Statistical analyses were conducted in GraphPad Prism 8 (GraphPad Software, San Diego, CA). Data were tested for normality by D'Agostino & Pearson Omnibus Normality Test. Since data analyzed in this study were not normally distributed, Mann-Whitney tests were used to compare two independent groups or Kruskal-Wallis tests with Dunn's Multiple Comparison adjustment were used to compare three or more groups. For multiple comparisons, comparisons were made between the following groups: 4-week anti-IL-10 vs. 4-week control, 8-week anti-IL-10 vs. 8-week control, 4-week anti-IL-10 vs. 8-week anti-IL-10, and 4-week control vs. 8-week control. Wilcoxon signed rank test was used to analyze matched pairs data. Fisher's exact test was used to analyze contingency tables. P-values ≤ 0.05 were considered significant, p-values ≤ 0.1 or those with statistically significant Kruskal-Wallis p-values were noted in individual graphs.

Computational modeling with *GranSim*

All simulations utilize our two-dimensional (2D) hybrid agent-based model (ABM), *GranSim* (62, 63). The model captures environmental, cellular, and bacterial dynamics across molecular, cellular, and tissue-scale events. *GranSim* has been calibrated extensively to data from a nonhuman primate model of TB and used to simulate a range of outcomes at the granuloma scale (20, 64, 65). At the molecular scale, *GranSim* incorporates cytokine and chemokine diffusion, secretion, and degradation. *GranSim* also tracks individual immune cells on a 2D simulation grid of microcompartments, including four macrophage states (resting, activated, infected, and chronically infected) and T cell types (cytotoxic, IFN-γ producing, and regulatory), fibroblasts and myofibroblasts. Granuloma formation at the tissue level is an emergent behavior of *GranSim.* See http://malthus.micro.med.umich.edu/GranSim for full model details and an executable file. We previously published model of fibrosis in the granuloma (65). In this study, we updated the fibrosis model to include a new rule regarding collagen, which is only produced by myofibroblasts. In this version of *GranSim* collagen blocks the migration and recruitment of cells into that specific grid compartment to more accurately capture the effect of fibrosis in the granuloma. The model was recalibrated to exhibit the expected phenomena with this new rule in place.

Computational platform and post-run analysis

GranSim is constructed through use of the C++ programming language, Boost libraries (distributed under the Boost software license; https://www.boost.org), and the Qt framework for visualization (distributed under General Public License). The ABM is cross-platform (Macintosh, Windows, Unix) and runs with or without visualization software. *GranSim* model simulations were performed on the XSEDE super computer (see Acknowledgments).

We used uncertainty and sensitivity analysis techniques to explore model parameter space. In particular, we used Latin hypercube sampling (LHS) (66, 67) to generate 1000 parameter sets by varying a range of input parameters that are listed in Supplemental Table 2. We then simulated the model with each parameter set for three replications with IL-10 present, and three with IL-10 removed from the system, for a total time of 150 days, yielding 6000 virtual granulomas, 3000 with IL-10 and 3000 without. The parameter sets resulted in a range of biologically feasible IL-10 concentrations in lungs, as well as a virtual library of in silico granulomas that are representative in the range of what we see *in vivo* (reducing the total number to 636 granulomas. We performed *virtual IL-10 depletion* experiments (IL-10 KOs) by setting all of the secretion rates of IL-10 to zero at the start of the simulation run. In our analysis, simulations were grouped by the concentration of IL-10 on the grid at the 150-day time point using quartiles. To identify important mechanisms driving the outcomes of interest we performed a sensitivity analysis using Partial Rank Correlation Coefficients (PRCCs). Correlations were calculated longitudinally to assess the correlation between parameters and outcomes of interest using the *spartan* package for *R* (68, 69). PRCCs represent correlations between −1.0 and 1.0, with higher magnitudes representative of higher correlations.

Results

Anti-IL-10 antibody neutralizes activity of macaque IL-10

The role of IL-10 in Mtb infections has been difficult to discern due to experimental model variability and technical difficulties in studying IL-10 at the local sites of infection in TB patients. To better understand IL-10 in TB lung granulomas, the primary site of infection, we used a cynomolgus macaque model of Mtb, which recapitulates granuloma structure and disease pathology observed in humans. We developed an antibody to specifically bind to macaque IL-10 (see Materials and Methods section), which neutralizes active IL-10 *in vitro* (Figure 1A). As an assay for IL-10 activity, we used D36 mouse mast cells that are IL-10-dependent for their proliferation, i.e. the addition of 20 ng/ml rhesus macaque IL-10 increases cell proliferation (70). The anti-macaque-IL-10 antibody added to the rhesus macaque IL-10 at varying concentrations reduced D36 mast cell proliferation to baseline levels, demonstrating neutralization of macaque IL-10 by this antibody. We used this anti-IL-10 antibody for all experiments in this study to investigate whether IL-10 had an effect on immune cell function in TB granulomas.

Immune responses in individual granulomas, even from the same macaque, are extremely variable (15) and not all have detectable levels of IL-10 (Figure 1B), thus we first aimed to understand whether neutralization of IL-10 affects T cell responses in lung granulomas *ex vivo*. Single cell suspensions of individual granulomas were either divided and treated with anti-IL-10 antibody or used as a media only control. In granulomas with detectable levels of IL-10 by ELISA, incubation with anti-IL-10 antibody *ex vivo* significantly increased the frequency of CD3+ T cells producing IL-2 compared to the media control (Figure 1C), with a trend towards increased IFN-γ and IL-17 T cell responses, suggesting that IL-10 in granulomas may suppress pro-inflammatory cytokine responses.

IL-10 neutralization during early Mtb infection in a NHP model

To confirm and expand upon our *ex vivo* IL-10 neutralization results, we conducted an *in vivo* IL-10 neutralization study (Figure 1D). We neutralized IL-10 during either the first 4 or 8 weeks of infection, beginning one day before Mtb infection and maintaining IL-10 neutralization with infusions of anti-IL-10 antibody every 10 days. A dose of 15mg/kg was chosen based on unpublished data from a similar human antibody in cynomolgus macaques, which indicated effectiveness without adverse side effects (David Sacks, personal communication). Lack of IL-10 can cause intestinal inflammation and colitis in human genetic studies and animal models (71-73). The Mtb-infected cynomolgus macaques treated with the anti-IL-10 antibody in this study did not have changes in stool, and histologic examination of intestines revealed no abnormal findings.

Reduced inflammation in granulomas early in Mtb infection

We tracked infection progression and inflammatory response in the lungs over the course of Mtb infection using PET-CT imaging with ^{18}F-FDG as a marker of inflammation (59). Overall lung inflammation (total FDG activity) was similar between the anti-IL-10 treated animals and the untreated control animals (Figure 2A), and a similar number of granulomas were found by PET-CT at 4 weeks post-infection in both groups, indicating no difference in establishment of infection. Although both groups had a range of FDG avidity in individual granulomas, a significantly higher frequency of granulomas from the IL-10 neutralized animals had very low FDG avidity (< 5 SUVR) at the 3–4 week time points [anti-IL-10: 11/58 (19.0%) FDG < 5 SUVR granulomas in the 8 week infection cohort, vs control: 3/54 (5.6%); Fisher's Exact Test p = 0. 0445) (Figure 2B). By 8 weeks post-infection, the control granulomas had returned to lower FDG activity values, more comparable to the granulomas in the anti-IL-10 group which did not change substantially between 4 and 8 weeks post-infection (Figure 2B). Since ^{18}F-FDG is a marker of metabolic activity and a general indicator of inflammation (58, 74), these results suggest that IL-10 may be indirectly or directly influencing inflammation at an early time point in a subset of granulomas.

Neutralization of IL-10 may decrease bacterial burden, but does not affect early infection outcome

We assessed the granulomas with early (3–4 weeks) low SUVR (Figure 2B) for bacterial burden at 8 weeks (necropsy) and found a significantly lower CFU/granuloma in the subset of low SUVR granulomas in both IL-10 neutralized and control groups as compared to granulomas with SUVR ≥ 5 (Figure 2C). This suggests that IL-10 neutralization had early effects on reducing inflammation in granulomas, which resulted in lower CFU in that subset of lesions by 8 weeks. However, these observed differences in a subset of individual granulomas did not translate to differences in overall infection outcome. Anti-IL-10 treated and untreated animals had similar gross pathology at 4 and 8 weeks post-infection (Figure 2D). Total thoracic (lung plus thoracic lymph node) bacterial burden, as well as bacterial burden within all individual granulomas, was also similar between the two groups at both 4 and 8 weeks post-infection (Figure 2E-F).

IL-10 does not alter immune cell composition of lung granulomas

Frequencies of cell populations and functionalities in lung granulomas were assessed by flow cytometry to determine whether neutralization of IL-10 influenced the local immune environment. Overall, the cell populations within granulomas were similar between the two groups at 4 and 8 weeks post-infection (Figure 3). There were no differences between IL-10 neutralized and control granulomas in terms of regulatory T cell populations (CD4+FOXP3+) and activated T cells (CD69+), with similar changes between 4 and 8 weeks within each group.

Since neutralization of IL-10 in TB granulomas *ex vivo* increased T cell cytokine responses, particularly IFN-γ, IL-2, and IL-17, we assessed whether anti-IL-10 antibody infusions *in vivo* also increased T cell cytokine responses. While Th1 (IFN-γ+ and/or TNF+) and IL-2+ T cell frequencies increased over infection time, there were no significant differences between anti-IL-10 treated and untreated animals (Figure 3). As we had observed *ex vivo*, granulomas from anti-IL-10 treated animals had higher frequencies of IL-17-producing T cells compared to granulomas from control animals 8 weeks after Mtb infection. Similar to our *ex vivo* results, the increase in CD3+ IL-17+ frequency was not consistent for all granulomas, suggesting that IL-10 may be affecting Th17 cells in a subset of TB granulomas.

Macrophages and B cells may be more responsive to IL-10 neutralization in lung granulomas

Since there were minimal differences in the T cell populations or their cytokine responses within lung granulomas (with the exception of IL-17), we sought to characterize which cells in TB granulomas express IL-10 receptor and would be responsive to IL-10. Immunohistochemistry revealed that the majority of cells in granulomas expressing IL-10 receptor (IL-10R) were not CD3+ T cells (Figure 4A-B). Instead, IL-10R co-localized with CD11c+ macrophage clusters on the outer edge of the granuloma macrophage region and with CD20+ B cells in the lymphocyte cuff (Figure 4A-C). Although IL-10 has been reported to have immunosuppressive effects on T cells (which may be indirect), it is possible that the T cells in granulomas are not the primary target of IL-10 since they tend to be the minor IL-10R-expressing immune cell in the granuloma. Thus, IL-10 neutralization may have a more significant role on the immune response of non-T cells in granulomas, such as macrophages and B cells.

To detect the effects of IL-10 neutralization on all cytokine-producing (innate and adaptive) cells within granulomas, total concentrations of cytokines within granuloma homogenates were measured by multiplex assay. At 4 weeks post-infection, granulomas from anti-IL-10 treated animals had significantly higher levels of IL-2, IL-13, IL-12p70, and IL-23 compared to granulomas from control animals (Figure 5). These cytokines are likely produced by innate cells and T cells. Neutralization of IL-10 did not lead to increases in all cytokine responses. Granulomas from anti-IL-10-treated animals had lower levels of IL-18 compared to granulomas from control animals (Figure 5).

The cytokine profile within granulomas changed by 8 weeks post-infection. Cytokines in granuloma homogenates at 4 weeks post-infection were no longer detectable or were no longer significantly different between granulomas of anti-IL-10 and untreated animals (Figure 5). Instead, granulomas from anti-IL-10 treated animals had significantly lower levels of IL-1β, IL-1RA, IL-6, and IFN-β compared to granulomas from untreated animals. These data suggest that IL-10 effects may be temporal, with inhibition of innate and adaptive immune responses in lung granulomas early in infection but enhancement of innate cytokine responses after 8 weeks of infection.

IL-10 inhibits cell recruitment and immune response within lymph nodes

Since thoracic lymph nodes (LNs) are also infected during Mtb infection (75) and there was an increase in T cell-promoting cytokines, such as IL-2 and IL-12p70, in the absence of IL-10 at 4 weeks post-infection, we investigated whether IL-10 neutralization affected the T cell response within LNs. At 4 weeks post-infection, the Mtb-infected LNs of anti-IL-10 treated animals had higher levels of bacterial burden compared to control animals (Figure 6A). Along with a higher bacterial burden, these Mtb-infected LNs had skewed CD4+/CD4− T cell ratios (anti-IL-10 median = 0.53, IQ_1 = 0.48, IQ_3 = 0.74; control median = 1.1, IQ_1 = 0.91 - IQ_3 = 1.49) (Figure 6B). There were 4-fold more CD4− (likely CD8+, although an antibody for CD8 was not used) CD3+ T cells in LNs of anti-IL-10 treated animals (median = 1.3×10^7 cells, IQ_1 = 7.68×10^6 - IQ_3 = 2.57×10^7) compared to control animals (median = 3.6×10^6 cells, IQ_1 = 2.43×10^6 - IQ_3 = 5.53×10^6), while numbers of CD4+ T cells were similar between both groups (anti-IL-10 median = 6.4×10^6 cells, IQ_1 = 4.08×10^6 - IQ3 = 1.8×10^7; control median = 4.1×10^6 cells, IQ_1 = 3.17×10^6 - IQ_3 = 6.95×10^6).

Although there were few effects of IL-10 neutralization on lymph node immune cell populations and T cell functionalities 4 weeks post-infection compared to lung granulomas (Figure 6C, Figure 3), the LN supernatants of the anti-IL-10 animals had higher levels of T cell-promoting cytokines IL-2, IL-13, and IL-12p70 and higher levels of IL-1β, IFN-γ and TNF compared to LNs of control animals (Figure 6D). There were also higher levels of lymphocyte-recruiting chemokines within LNs of anti-IL-10 animals (Figure 6E). Corresponding to increased bacterial burden, CD4− T cells, T cell-promoting cytokines, and lymphocyte-recruiting chemokines, there were more total immune cells and increased weights of LNs from anti-IL-10 animals as compared to controls (Supplemental Figure 1B, C). These data suggest that IL-10 may inhibit T cell proliferation and immune cell recruitment in LNs, particularly of CD4− T cells, during Mtb infection. However, the ability of IL-10 to directly or indirectly downregulate these immune responses and reduce CD4− T cells in the LN at 4 weeks may be beneficial for the initial Mtb control in LNs, as evidenced by the higher bacterial loads in LNs of anti-IL-10 treated animals at 4 weeks.

After an additional 4 weeks of Mtb infection, the patterns in bacterial burden and T cell ratios in LNs reversed compared to the earlier time point. At 8 weeks post-infection, LN bacterial burdens were similar between anti-IL-10 and control animals (Figure 6A). The ratio of T cell subsets in anti-IL-10 animals increased, with more CD4+ T cells relative to CD4− T cells (CD4+/CD4− ratio median = 1.9, IQ_1 = 1.647 - IQ_3 = 2.5) in the IL-10 neutralized group as compared to the control group (median = 0.98, IQ_1 = 0.5771 - IQ_3 =

1.456) (Figure 6B). While the number of CD4+ T cells in Mtb-infected LNs were similar at 4 and 8 weeks, the elevated numbers of CD4− T cells observed in anti-IL-10 treated animals 4 weeks of Mtb infection decreased by 8 weeks (median = 2.4×10^6 cells, $IQ_1 = 1.94\times10^6$ - $IQ_3 = 4.69\times10^6$), increasing the CD4+/CD4− ratio.

As in lung granulomas, there are significantly higher frequencies of T cells producing IL-17 in Mtb-infected LNs from anti-IL-10 treated animals compared to untreated animals at 8 weeks post-infection (Figure 6C). However, IL-10 neutralization did not affect other types of T cells (Supplemental Figure 1B) or total cytokine and chemokine production (Supplemental Table 1) within LNs of anti-IL-10 treated animals compared to untreated controls. By 8 weeks, there were also similar numbers of immune cells within LNs of anti-IL-10 treated as compared to control animals (Supplemental Figure 1C). Taken together, these results suggest that IL-10 may help initially control bacterial growth within LNs and prevent excessive T cell proliferation and recruitment within the first 4 weeks of Mtb infection, but may have fewer effects on the LNs after 8 weeks of infection.

IL-10 neutralization leads to increased collagenization and fibrosis in lung granulomas

Besides the immunological changes occurring in lung granulomas and Mtb-infected LNs in the absence of IL-10, there were changes in lung granuloma structure from anti-IL-10-treated animals. Blinded histopathological analysis of lung granulomas from both treatment groups revealed more evidence of fibrosis within granulomas from animals treated with anti-IL-10 compared to control animals at the time of necropsy (Figure 7A). In general, the presence of fibrosis is relatively unusual in early infection granulomas. However, 26% of granulomas analyzed from anti-IL-10 animals showed signs of fibrosis, as compared to <5% in control animals, which suggests that IL-10 impairs healing-associated fibrosis in lung granulomas during Mtb infections.

To further understand these histopathological changes, Masson’s trichrome staining was used to compare collagen levels in a random subset of granulomas from the anti-IL-10 treated and untreated animals at both time points. After 8 weeks of infection, granulomas from anti-IL-10 treated animals had slightly higher collagen (blue) mean pixel intensity compared to untreated controls and compared to IL-10 neutralized granulomas at 4 weeks of infection (Figure 7B-C). We examined the collagen deposition in lung granulomas more closely, using immunohistochemistry staining specifically against collagen I. While most granulomas had some collagen I, lung granulomas from anti-IL-10 treated animals, especially by 8 weeks, often had more infiltrative collagen patterns into the central necrotic caseous area of the granuloma (Figure 7C, Collagen I-CD68-CD163 insets). We did not observe differences in fibroblast (vimentin-positive) or myofibroblast (alpha-SMA-positive) cells between granulomas from anti-IL-10 treated and untreated control animals, although we identified vimentin- and alpha-SMA-positive cells in some of the granulomas (Figure 7C, Vimentin-CD68-alpha-SMA).

In other models, IL-10 has been suggested to have an indirect effect on fibrosis through other cytokine pathways; two of the best characterized cytokine mediators of fibrosis are TGF-β and Th2 cytokines IL-4/IL-13 (76). In support of this, IL-13 was increased within lung granulomas from anti-IL-10 treated animals after 4 weeks of Mtb infection (Figure 5),

while IL-4 was not detectable (Supplemental Table 1). Using phospho-SMAD3 and phospho-STAT6 to detect TGF-β or IL-4/IL-13 signaling within granulomas, respectively, we observed signaling through both pathways under both treatments at both time points, with no discernable differences based on presence of IL-10 or infection times (Figure 7C). Thus, during Mtb infection, IL-10 may normally suppress early collagenization and fibrosis within lung granulomas, possibly through inhibition of IL-13, although the pathways leading to granuloma fibrosis during Mtb infection need further investigation.

Simulated granulomas capture complexity and range of IL-10 concentrations in NHP TB granulomas

Although we observed immunological and structural changes in both lung granulomas and LNs during Mtb infection when IL-10 was neutralized, these changes did not alter overall disease outcomes, according to our outcome measures. Due to the short nature of our *in vivo* study (8 weeks), we used computational modeling to explore the role of IL-10 on granuloma function during longer term infections using *GranSim*, our next-generation agent-based model (ABM) (77). We used Latin Hypercube Sampling (LHS, see Materials and Methods) to simulate thousands of biologically feasible individual granulomas and simulated these in both virtual wild-type (control) and IL-10 depleted (IL-10 Knockout, KO) scenarios. Representative snapshots of WT and IL-10 KO granulomas, along with bar charts of cellular compositions are shown in Figure 8A. The parameters we varied included several that affect the concentration of IL-10 within a granuloma (Supplemental Table 2 shows the list of parameters and the ranges used). We first verified using LHS that varying selected parameters resulted in a range of IL-10 concentrations within the granuloma was qualitatively similar to those observed *in vivo* for WT and also created the IL-10 KO simulations (Figure 8B-C).

We then performed a sensitivity analysis using partial-rank correlation coefficients (PRCCs, see Materials and Methods) to determine the most significantly correlated parameters (mechanisms) within a granuloma environment that were affected during the simulated IL-10 KO. Supplemental Figure 2 shows the longitudinal PRCCs for parameters that are significantly correlated with IL-10 in the granuloma environment at one or more time points ($p < 0.05$). Our analyses predict that early during infection, the amount of IL-10 secreted by infected macrophages, and the maximum amount of TGF-β required to inhibit macrophage phagocytic activity by 50% are the most influential mechanisms affecting the concentration of IL-10 in the granuloma environment. Starting from 6 weeks post-infection, T cell-related mechanisms become the most significant of all of the varied parameters related to controlling IL-10 concentrations in a granuloma. The sensitivity analysis also suggests that granulomas with higher IL-10 are associated with fewer IFN-γ-producing T cells and more regulatory T cells. This follows from the PRCC values shown in Supplementary Fig. 2, as threshold parameters when low allow more recruitment (e.g. Treg-thresholdRec) and Recruitment probabilities when low allow little to no recruitment of cells (Tgam maxRecProb).

It should also be noted that in our model the role of TGF-βcould be inflated due to the lack of IL-13 in the computational model that would complement the role of TGF-β*in vivo*.

GranSim predicts that long-term depletion of IL-10 reduces bacterial burden and increases rate of lesion sterilization

Consistent with what we have previously observed using our computational model, depleting IL-10 affects the numbers of granulomas that sterilize over the course of infection (20, 78). Figure 9A demonstrates 63% of simulated granulomas were sterilized in the IL-10 KO simulations after 150 days (dashed black line), compared to 51% of granulomas in the control group (WT, solid black line).

To further explore the role of IL-10, we grouped the WT simulations into 4 groups by quartiles of IL-10 concentrations at 4-weeks post infection (Figure 9A). To eliminate bias, we first confirmed that the average time to sterilization was not less than the 4-week time point that we used for grouping (Figure 9B). Our results demonstrate that granulomas with the lowest IL-10 concentrations at four weeks post infection (<25%, blue and 25 – 50%, yellow) had similar frequencies of sterilization by 20 weeks as the IL-10KO granulomas. However, granulomas in the higher IL-10 concentration groups at 4 weeks post-infection (50–75%, green and >75%, red) were less likely to sterilize at 150 days than those with lower IL-10 concentrations or the IL-10KO (Figure 9A). The time to sterilization was not significantly altered between IL-10 groups, except that there was a higher number of very early (less that one week) sterilizing simulated granulomas in the lowest IL-10 group (<25%, blue) and the IL-10 KOs. These represent early clearance of Mtb before granuloma formation, suggesting animals with little or no IL-10 may have fewer granulomas as compared to animals with naturally higher IL-10 concentrations in the lung. However, these slight differences predicted from the computational model would be difficult to observe *in vivo* without larger numbers of animal studies.

Discussion

Although pro-inflammatory cytokines have been demonstrated to be necessary to control Mtb replication, the role of anti-inflammatory cytokines to counteract potentially tissue-damaging cytokines have not been fully elucidated. Previous studies resulted in contradictory conclusions about the beneficial or harmful roles of IL-10 during Mtb infection (15, 42-53), with some suggesting that IL-10 may have differential roles depending on stage of infection (42, 43, 49). We sought to clarify the role of IL-10 within TB lung granulomas using a NHP model of TB and an anti-IL-10 antibody to neutralize macaque IL-10. Our *in vivo* study neutralizing the effects of IL-10 in a cohort of NHPs demonstrated that IL-10 may increase inflammation in some lung granulomas and decrease cytokine responses within lung granulomas and lymph nodes very early (4 weeks) in Mtb infection, but with reduced effects by 8 weeks of Mtb infection. IL-10 may also affect the structure of lung granulomas, reducing early collagenization and fibrosis. While IL-10 may influence the local environment of a subset of lung granulomas and lymph nodes, the presence or absence of IL-10 did not ultimately influence the overall bacterial burden or disease pathology in the host, at least during the early stages of infection.

For technical reasons, it was only feasible to neutralize IL-10 *in vivo* for several weeks; thus, we were unable to investigate the effects of longer neutralization on infection outcome. Computational modeling provided the opportunity to investigate the effects of long term

depletion of IL-10 in granulomas. In previously published computational modeling studies, we demonstrated that depleting IL-10 can increase the probability that a granuloma is cleared in NHPs and identified activated macrophages as the major IL-10 producers within a TB granuloma, affecting the CFU in a granuloma (20). In this study we extended our previous work to explore the effect IL-10 has on CFU, sterilization, and development of fibrosis by using a next-generation version of *GranSim*, our previously published ABM of cellular dynamics in the lung (65). Our results in this system suggest that depletion of IL-10 decreases the overall numbers of granulomas, increases the probability of a granuloma sterilizing, and contributes to increased fibrosis by enhancing fibroblast proliferation and fibroblast to myofibroblast differentiation.

A limitation to our study was that we were unable to accurately quantify the concentration of anti-IL-10 antibody in the tissues or to measure the pharmacokinetics of this particular antibody, thus our neutralization of IL-10 in the tissues may not have been optimal at all time points. Despite this, we were able to identify immunologic and pathologic effects of the antibody within the lung and lymph node tissues in the NHP *in vivo* experiments, where the anti-IL-10 antibody had the greatest effect on the host immune response to Mtb infection within the first weeks of infection. A subset of granulomas from anti-IL-10 treated animals had lower inflammation (FDG SUV<5) early in infection (4 weeks), which corresponded to significantly lower CFU 4 weeks later. Anti-IL-10 treatment also led to increased cytokine response in lung granulomas and LNs at 4 weeks, particularly in the pro-inflammatory cytokines IL-23, IL-2, IL-12p70, IFN-γ, and TNF. These results support previous *in vitro* and *in vivo* experiments that noted increased pro-inflammatory cytokine response, particularly in macrophages and T cells, with the blockade or removal of IL-10 (33, 35, 36). IL-10 can affect most immune cells, but it may primarily affect myeloid cells in the context of Mtb infection (46, 49). Many of the T cell-promoting cytokines and chemokines that were increased in anti-IL-10 treated animals at 4 weeks post-infection are produced by myeloid cells and there were lower concentrations of macrophage-produced cytokines (IL-1β, IL-1RA, IL-6, IFN-β) in lung granulomas of anti-IL-10 treated animals at 8 weeks. In addition, as we show here and others have demonstrated, the receptor for IL-10 (IL-10R) is predominantly on non-T cells, especially in TB granulomas (48, 78).

While we observed increased T cell-promoting cytokines and chemokines in lung granulomas and LNs in anti-IL-10 animals, we did not observe corresponding increased T cell activity in lung granulomas; however, there were altered T cell populations in LNs, as reported in other TB studies (43, 45). Unlike Redford et al., who observed increased numbers of CD4+ T cells in the draining LNs of IL-10 KO mice compared to controls (45), we observed an increased number of CD4− (presumably CD8+) T cells, particularly at 4 weeks post-infection. Instead, our results were similar to acute LCMV infections, where CD8+ T cells increased during IL-10 blockade, particularly during the priming phase (79, 80); similar results were also seen with listeria and HIV infections (81, 82). However, the heightened LN T cell responses did not translate into improved host control of Mtb infection by 8 weeks.

The absence of IL-10 in this study increased fibrosis in lung granulomas. Although some studies have suggested that IL-10 may act directly on fibroblasts to increase collagen

deposition in the skin, IL-10 is generally thought to reduce fibrosis through modulation of other pro-fibrotic cytokines (76, 83-85). There were increased concentrations of IL-13 at 4 weeks and increased frequencies of T cells producing IL-17 in lung granulomas of anti-IL-10 treated animals. Both IL-13 and IL-17 have been demonstrated to be critical contributors to fibrosis in other models (76, 86, 87). Other potential mediators of fibrosis, IL-12, IL-1 family (IL-1β, IL-1RA, IL-18), IL-6, IL-23, and IFN-β (86, 88-91), were also dysregulated during IL-10 neutralization in this study. Our study only provided snapshots of IL-10 neutralization during early Mtb infection, thus we were unable to pinpoint mechanisms of increased fibrosis in this study, although our computational work indicated TGF-β as a critical factor for fibrosis in the absence of IL-10.

The role of fibrotic lesions in TB is unclear, but fibrosis tends to be associated with containment, drug treatment, and sterility (92, 93). Fibrosis is a healing response that can result in pathology but can also limit spread of infection. It is not generally observed at early time points in Mtb infection, but becomes more common during longer infections. Early blockade of IL-10 during Mtb infection led to fibrotic granulomas and a complete lack of IL-10 led to granuloma structure changes in the mouse model (43, 50). While we did not observe the same levels of bacterial control in our NHP model early in Mtb infection, neutralization of IL-10 increased the fibrosis and collagenization of lung granulomas, and our computational modeling of IL-10KO suggested increased bacterial control over extended infection times. The mediators and significance of fibrosis in granulomas are currently unclear, but fibrosis in lung granulomas may lead to improved bacterial containment and/or modified lung pathology in the long term beyond the scope of this study. However, this raises the possibility that neutralization of IL-10 during drug treatment could be a potential host-directed therapy for increasing response to drug treatment in active TB, although this would require further testing.

The transient increases in immune responses in lung granulomas and lymph nodes with IL-10 neutralization did not affect overall disease pathology or bacterial burden in the host during early infection as other studies had suggested (42, 43, 45), but it also did not increase disease pathology and decreased survival (50). There are several possibilities to explain these findings. First, IL-10 may not have a significant role in the host immune response to Mtb, as supported by a subset of the published murine studies (50-52, 94). Second, not all granulomas may respond to IL-10 in the same manner. Previous studies from our lab have demonstrated the individuality of each granuloma, even from the same animal (15, 58). Our *ex vivo* neutralization assays also suggest that granulomas may not all be producing or responding to IL-10 during Mtb infection. Third, other host factors may compensate for the lack of IL-10. Roach et al. showed a transient decrease in bacterial burden of IL-10 knock-out mice after 4 weeks of infection, but by 8 weeks post-infection, there was no difference in bacterial burden compared to wild-type mice (53). Other studies also showed that the combination of T cell and innate cell production of IL-10 were critical for Mtb protection (46, 49). In our study, we observed greater changes in the cytokine and chemokine response in anti-IL-10 animals after 4 weeks of infection, which could be due to the onset of the adaptive immune response counteracting and minimizing the influence of IL-10 by 8 weeks (11). The observed increase in the Th2 cytokine IL-13 with anti-IL-10 treatment at 4 weeks post-infection may have helped compensate for the lack of IL-10. Although we quantified

FOXP3+ regulatory T cells and assessed TGF-β signaling by immunohistochemistry and computational modeling in our study, we were unable to quantify the anti-inflammatory cytokine TGF-β. Mtb can also stimulate the production of TGF-β, which could compensate for the lack of IL-10 (78, 95). Due to the limitations of this study, we may not have assessed factor(s) that could compensate for the actions of IL-10.

Finally, the role of IL-10 during Mtb infection could be time-dependent. The *in vivo* study was restricted to the first 8 weeks of infection to capture the change in innate and adaptive immune responses. Turner et al. observed overexpression of IL-10 in the mouse model of Mtb infection had no effect on the bacterial load until 5 months post-infection (47). Other studies found that IL-10 had the greatest effect on the host ability to control the bacterial burden starting at least after 3 months of infection (42, 43, 48). Moreira-Texeira et al. observed significantly lower bacterial burdens in IL-10-depleted Mtb-infected mice after two months, but not within one month of infection (46). Thus, early IL-10 neutralization may initiate the immune response for long-term control of bacterial loads outside the scope of our *in vivo* study, as suggested by our *in silico* computational modeling of IL-10 and previously by Cyktor et al. (43). Future studies investigating the role of IL-10 during chronic Mtb infections are warranted.

Overall, neutralization of IL-10 in macaques during Mtb infection altered the innate and adaptive immune responses within the local granuloma and lymph node environments but did not result in improved infection outcome. We also did not observe excessive inflammation in the absence of IL-10. Thus, IL-10 alone may not have a significant role in early Mtb infections, likely having greater effects in cooperation with other immune cells/cytokines (78, 95, 96). This study further demonstrates the need for a properly balanced immune response within the locally affected tissues during Mtb infection and the need to continue to identify other host factors that may inhibit effective immune responses against Mtb (97).

Supplementary Material

Refer to Web version on PubMed Central for supplementary material.

Acknowledgments:

Rhesus IL-10 was kindly provided by Dr. Francois Villinger. We thank Dr. David Sacks (NIH NIAID) for helpful discussions regarding study design. We are grateful to the members of the Flynn, Scanga, Lin and Mattila labs for advice and discussion regarding this work.

This research was supported by R01AI123093 and R01HL110811 awarded to DEK and JLF. Any simulations also use resources of the National Energy Research Scientific Computing Center, which is supported by the Office of Science of the U.S. Department of Energy under Contract No. ACI-1053575 and the Extreme Science and Engineering Discovery Environment (XSEDE), which is supported by National Science Foundation grant MCB140228. EAW was supported on NIH T32 AI060525 and SE was supported by an Intersect Fellowship from the American Association of Immunologists

References

1. WHO. Tuberculosis Fact Sheet.

2. Clay H, Davis JM, Beery D, Huttenlocher A, Lyons SE, and Ramakrishnan L. 2007 Dichotomous role of the macrophage in early Mycobacterium marinum infection of the zebrafish. Cell host & microbe 2: 29–39. [PubMed: 18005715]

3. Tsai MC, Chakravarty S, Zhu G, Xu J, Tanaka K, Koch C, Tufariello J, Flynn J, and Chan J. 2006 Characterization of the tuberculous granuloma in murine and human lungs: cellular composition and relative tissue oxygen tension. Cellular microbiology 8: 218–232. [PubMed: 16441433]

4. Srivastava S, Ernst JD, and Desvignes L. 2014 Beyond macrophages: the diversity of mononuclear cells in tuberculosis. Immunological reviews 262: 179–192. [PubMed: 25319335]

5. Wolf AJ, Linas B, Trevejo-Nuñez GJ, Kincaid E, Tamura T, Takatsu K, and Ernst JD. 2007 Mycobacterium tuberculosis infects dendritic cells with high frequency and impairs their function in vivo. The Journal of Immunology 179: 2509–2519. [PubMed: 17675513]

6. Wolf AJ, Desvignes L, Linas B, Banaiee N, Tamura T, Takatsu K, and Ernst JD. 2008 Initiation of the adaptive immune response to Mycobacterium tuberculosis depends on antigen production in the local lymph node, not the lungs. Journal of Experimental Medicine 205: 105–115. [PubMed: 18158321]

7. Chackerian AA, Alt JM, Perera TV, Dascher CC, and Behar SM. 2002 Dissemination of Mycobacterium tuberculosis is influenced by host factors and precedes the initiation of T-cell immunity. Infection and immunity 70: 4501–4509. [PubMed: 12117962]

8. Lin PL, Rodgers M, Smith L, Bigbee M, Myers A, Bigbee C, Chiosea I, Capuano SV, Fuhrman C, Klein E, and Flynn JL. 2009 Quantitative comparison of active and latent tuberculosis in the cynomolgus macaque model. Infection and immunity 77: 4631–4642. [PubMed: 19620341]

9. Kahnert A, Höpken UE, Stein M, Bandermann S, Lipp M, and Kaufmann SH. 2007 Mycobacterium tuberculosis triggers formation of lymphoid structure in murine lungs. The Journal of infectious diseases 195: 46–54. [PubMed: 17152008]

10. Phuah JY, Mattila JT, Lin PL, and Flynn JL. 2012 Activated B cells in the granulomas of nonhuman primates infected with Mycobacterium tuberculosis. The American journal of pathology 181: 508–514. [PubMed: 22721647]

11. Cadena AM, Flynn JL, and Fortune SM. 2016 The importance of first impressions: early events in mycobacterium tuberculosis infection influence outcome. MBio 7: e00342–00316. [PubMed: 27048801]

12. Dannenberg AM Jr 1989 Immune mechanisms in the pathogenesis of pulmonary tuberculosis. Reviews of infectious diseases 11: S369–S378. [PubMed: 2496453]

13. Flynn JL, and Chan J. 2001 Immunology of tuberculosis. Annual review of immunology 19: 93–129.

14. O'Garra A, Redford PS, McNab FW, Bloom CI, Wilkinson RJ, and Berry MP. 2013 The immune response in tuberculosis. Annual review of immunology 31: 475–527.

15. Gideon HP, Phuah J, Myers AJ, Bryson BD, Rodgers MA, Coleman MT, Maiello P, Rutledge T, Marino S, Fortune SM, Kirschner DE, Lin PL, and Flynn JL. 2015 Variability in tuberculosis granuloma T cell responses exists, but a balance of pro- and anti-inflammatory cytokines is associated with sterilization. PLoS pathogens 11: e1004603. [PubMed: 25611466]

16. Poulsen A 1950 Some clinical features of tuberculosis. 1. Incubation period. Acta tuberculosea Scandinavica 24: 311. [PubMed: 14783027]

17. POULSEN A 1957 Some Clinical Features of Tuberculosis Pts. 2–7. Acta tuberculosea Scandinavica 33: 37–92. [PubMed: 13424392]

18. Coleman MT, Maiello P, Tomko J, Frye LJ, Fillmore D, Janssen C, Klein E, and Lin PL. 2014 Early Changes by (18)Fluorodeoxyglucose Positron Emission Tomography Coregistered with Computed Tomography Predict Outcome after Mycobacterium tuberculosis Infection in Cynomolgus Macaques. Infection and immunity 82: 2400–2404. [PubMed: 24664509]

19. Lin PL, Ford CB, Coleman MT, Myers AJ, Gawande R, Ioerger T, Sacchettini J, Fortune SM, and Flynn JL. 2013 Sterilization of granulomas is common in active and latent tuberculosis despite within-host variability in bacterial killing. Nature medicine.

20. Cilfone NA, Ford CB, Marino S, Mattila JT, Gideon HP, Flynn JL, Kirschner DE, and Linderman JJ. 2015 Computational modeling predicts IL-10 control of lesion sterilization by balancing early

host immunity–mediated antimicrobial responses with caseation during Mycobacterium tuberculosis infection. The Journal of Immunology 194: 664–677. [PubMed: 25512604]

21. Bean AG, Roach DR, Briscoe H, France MP, Korner H, Sedgwick JD, and Britton WJ. 1999 Structural deficiencies in granuloma formation in TNF gene-targeted mice underlie the heightened susceptibility to aerosol Mycobacterium tuberculosis infection, which is not compensated for by lymphotoxin. The Journal of Immunology 162: 3504–3511. [PubMed: 10092807]
22. Casanova J-L, and Abel L. 2002 Genetic dissection of immunity to mycobacteria: the human model. Annual review of immunology 20: 581–620.
23. Cooper AM, Dalton DK, Stewart TA, Griffin J, Russell D, and Orme I. 1993 Disseminated tuberculosis in interferon gamma gene-disrupted mice. The Journal of experimental medicine 178: 2243–2247. [PubMed: 8245795]
24. Flynn JL, Chan J, Triebold KJ, Dalton DK, Stewart TA, and Bloom BR. 1993 An essential role for interferon gamma in resistance to Mycobacterium tuberculosis infection. The Journal of experimental medicine 178: 2249–2254. [PubMed: 7504064]
25. Flynn JL, and Ernst JD. 2000 Immune responses in tuberculosis. Current opinion in immunology 12: 432–436. [PubMed: 10899019]
26. Flynn JL, Goldstein MM, Chan J, Triebold KJ, Pfeffer K, Lowenstein CJ, Schrelber R, Mak TW, and Bloom BR. 1995 Tumor necrosis factor-α is required in the protective immune response against Mycobacterium tuberculosis in mice. Immunity 2: 561–572. [PubMed: 7540941]
27. Khader SA, Bell GK, Pearl JE, Fountain JJ, Rangel-Moreno J, Cilley GE, Shen F, Eaton SM, Gaffen SL, and Swain SL. 2007 IL-23 and IL-17 in the establishment of protective pulmonary CD4+ T cell responses after vaccination and during Mycobacterium tuberculosis challenge. Nature immunology 8: 369–377. [PubMed: 17351619]
28. Lin PL, Myers A, Smith LK, Bigbee C, Bigbee M, Fuhrman C, Grieser H, Chiosea I, Voitenek NN, and Capuano SV. 2010 Tumor necrosis factor neutralization results in disseminated disease in acute and latent Mycobacterium tuberculosis infection with normal granuloma structure in a cynomolgus macaque model. Arthritis & Rheumatism 62: 340–350. [PubMed: 20112395]
29. Lin PL, Plessner HL, Voitenok NN, and Flynn JL. 2007 Tumor necrosis factor and tuberculosis In Journal of Investigative Dermatology Symposium Proceedings. Elsevier 22–25.
30. Quesniaux VF, Jacobs M, Allie N, Grivennikov S, Nedospasov SA, Garcia I, Olleros ML, Shebzukhov Y, Kuprash D, and Vasseur V. 2010 TNF in host resistance to tuberculosis infection In TNF Pathophysiology. Karger Publishers 157–179.
31. Roach DR, Bean AG, Demangel C, France MP, Briscoe H, and Britton WJ. 2002 TNF regulates chemokine induction essential for cell recruitment, granuloma formation, and clearance of mycobacterial infection. The Journal of immunology 168: 4620–4627. [PubMed: 11971010]
32. Scriba TJ, Kalsdorf B, Abrahams D-A, Isaacs F, Hofmeister J, Black G, Hassan HY, Wilkinson RJ, Walzl G, and Gelderbloem SJ. 2008 Distinct, specific IL-17-and IL-22-producing CD4+ T cell subsets contribute to the human anti-mycobacterial immune response. The Journal of Immunology 180: 1962–1970. [PubMed: 18209095]
33. Couper KN, Blount DG, and Riley EM. 2008 IL-10: the master regulator of immunity to infection. The Journal of Immunology 180: 5771–5777. [PubMed: 18424693]
34. Sabat R, Grütz G, Warszawska K, Kirsch S, Witte E, Wolk K, and Geginat J. 2010 Biology of interleukin-10. Cytokine & Growth Factor Reviews 21: 331–344. [PubMed: 21115385]
35. Iyer SS, and Cheng G. 2012 Role of interleukin 10 transcriptional regulation in inflammation and autoimmune disease. Critical Reviews™ in Immunology 32.
36. Moore KW, de Waal Malefyt R, Coffman RL, and O'Garra A. 2001 Interleukin-10 and the interleukin-10 receptor. Annual review of immunology 19: 683–765.
37. Gerosa F, Nisii C, Righetti S, Micciolo R, Marchesini M, Cazzadori A, and Trinchieri G. 1999 CD4+ T cell clones producing both interferon-γ and interleukin-10 predominate in bronchoalveolar lavages of active pulmonary tuberculosis patients. Clinical Immunology 92: 224–234. [PubMed: 10479527]
38. Verbon A, Juffermans N, Van Deventer S, Speelman P, Van Deutekom H, and Van Der Poll T. 1999 Serum concentrations of cytokines in patients with active tuberculosis (TB) and after treatment. Clinical and experimental immunology 115: 110. [PubMed: 9933428]

39. Bonecini-Almeida MG, Ho JL, Boéchat N, Huard RC, Chitale S, Doo H, Geng J, Rego L, Lazzarini LCO, and Kritski AL. 2004 Down-modulation of lung immune responses by interleukin-10 and transforming growth factor β (TGF-β) and analysis of TGF-β receptors I and II in active tuberculosis. Infection and immunity 72: 2628–2634. [PubMed: 15102771]
40. Gong J-H, Zhang M, Modlin RL, Linsley PS, Iyer D, Lin Y, and Barnes PF. 1996 Interleukin-10 downregulates Mycobacterium tuberculosis-induced Th1 responses and CTLA-4 expression. Infection and immunity 64: 913–918. [PubMed: 8641800]
41. O'Leary S. n., O'Sullivan MP, and Keane J. 2011 IL-10 blocks phagosome maturation in Mycobacterium tuberculosis–infected human macrophages. American journal of respiratory cell and molecular biology 45: 172–180. [PubMed: 20889800]
42. Beamer GL, Flaherty DK, Assogba BD, Stromberg P, Gonzalez-Juarrero M, de Waal Malefyt R, Vesosky B, and Turner J. 2008 Interleukin-10 promotes Mycobacterium tuberculosis disease progression in CBA/J mice. The Journal of Immunology 181: 5545–5550. [PubMed: 18832712]
43. Cyktor JC, Carruthers B, Kominsky RA, Beamer GL, Stromberg P, and Turner J. 2013 IL-10 inhibits mature fibrotic granuloma formation during Mycobacterium tuberculosis infection. The Journal of Immunology 190: 2778–2790. [PubMed: 23396944]
44. Pitt JM, Stavropoulos E, Redford PS, Beebe AM, Bancroft GJ, Young DB, and O'Garra A. 2012 Blockade of IL-10 signaling during BCG vaccination enhances and sustains Th1, Th17, and innate lymphoid IFN-γ and IL-17 responses and increases protection to Mycobacterium tuberculosis infection. Journal of immunology (Baltimore, Md.: 1950) 189: 4079.
45. Redford PS, Boonstra A, Read S, Pitt J, Graham C, Stavropoulos E, Bancroft GJ, and O'Garra A. 2010 Enhanced protection to Mycobacterium tuberculosis infection in IL-10-deficient mice is accompanied by early and enhanced Th1 responses in the lung. European journal of immunology 40: 2200–2210. [PubMed: 20518032]
46. Moreira-Teixeira L, Redford PS, Stavropoulos E, Ghilardi N, Maynard CL, Weaver CT, do Rosário APF, Wu X, Langhorne J, and O'Garra A. 2017 T Cell–Derived IL-10 Impairs Host Resistance to Mycobacterium tuberculosis Infection. The Journal of Immunology 199: 613–623. [PubMed: 28584007]
47. Turner J, Gonzalez-Juarrero M, Ellis DL, Basaraba RJ, Kipnis A, Orme IM, and Cooper AM. 2002 In vivo IL-10 production reactivates chronic pulmonary tuberculosis in C57BL/6 mice. The Journal of Immunology 169: 6343–6351. [PubMed: 12444141]
48. Schreiber T, Ehlers S, Heitmann L, Rausch A, Mages J, Murray PJ, Lang R, and Hölscher C. 2009 Autocrine IL-10 induces hallmarks of alternative activation in macrophages and suppresses antituberculosis effector mechanisms without compromising T cell immunity. The Journal of Immunology 183: 1301–1312. [PubMed: 19561100]
49. Huynh JP, Lin C-C, Kimmey JM, Jarjour NN, Schwarzkopf EA, Bradstreet TR, Shchukina I, Shpynov O, Weaver CT, and Taneja R. 2018 Bhlhe40 is an essential repressor of IL-10 during Mycobacterium tuberculosis infection. Journal of Experimental Medicine 215: 1823–1838. [PubMed: 29773644]
50. Higgins DM, Sanchez-Campillo J, Rosas-Taraco AG, Lee EJ, Orme IM, and Gonzalez-Juarrero M. 2009 Lack of IL-10 alters inflammatory and immune responses during pulmonary< i> Mycobacterium tuberculosis infection. Tuberculosis 89: 149–157. [PubMed: 19213603]
51. Jung YJ, Ryan L, LaCourse R, and North RJ. 2003 Increased interleukin-10 expression is not responsible for failure of T helper 1 immunity to resolve airborne Mycobacterium tuberculosis infection in mice. Immunology 109: 295–299. [PubMed: 12757625]
52. North R 1998 Mice incapable of making IL-4 or IL-10 display normal resistance to infection with Mycobacterium tuberculosis. Clinical & Experimental Immunology 113: 55–58. [PubMed: 9697983]
53. Roach D, Martin E, Bean A, Rennick D, Briscoe H, and Britton W. 2001 Endogenous Inhibition of Antimycobacterial Immunity by IL-10 Varies between Mycobacterial Species. Scandinavian journal of immunology 54: 163–170. [PubMed: 11439163]
54. Presta LG 2011 Interleukin-10 antibodies In Google Patents, Australia.
55. Capuano SV, Croix DA, Pawar S, Zinovik A, Myers A, Lin PL, Bissel S, Fuhrman C, Klein E, and Flynn JL. 2003 Experimental Mycobacterium tuberculosis infection of cynomolgus macaques

closely resembles the various manifestations of human M. tuberculosis infection. Infection and immunity 71: 5831–5844. [PubMed: 14500505]

56. Lin PL, Pawar S, Myers A, Pegu A, Fuhrman C, Reinhart TA, Capuano SV, Klein E, and Flynn JL. 2006 Early events in Mycobacterium tuberculosis infection in cynomolgus macaques. Infection and immunity 74: 3790–3803. [PubMed: 16790751]
57. Cadena AM, Hopkins FF, Maiello P, Carey AF, Wong EA, Martin CJ, Gideon HP, DiFazio RM, Andersen P, and Lin PL. 2018 Concurrent infection with Mycobacterium tuberculosis confers robust protection against secondary infection in macaques. PLoS pathogens 14: e1007305. [PubMed: 30312351]
58. Lin PL, Coleman T, Carney JP, Lopresti BJ, Tomko J, Fillmore D, Dartois V, Scanga C, Frye LJ, and Janssen C. 2013 Radiologic responses in cynomolgus macaques for assessing tuberculosis chemotherapy regimens. Antimicrobial agents and chemotherapy 57: 4237–4244. [PubMed: 23796926]
59. White AG, Maiello P, Coleman MT, Tomko JA, Frye LJ, Scanga CA, Lin PL, and Flynn JL. 2017 Analysis of 18FDG PET/CT imaging as a tool for studying Mycobacterium tuberculosis infection and treatment in non-human primates. JoVE (Journal of Visualized Experiments): e56375.
60. Lin PL e. a. 2013 Radiologic Responses in Cynomolgus Macaques for Assessing Tuberculosis Chemotherapy Regimens. Antimicrob Agents and Chemotherapy 57: 8.
61. Maiello P, DiFazio RM, Cadena AM, Rodgers MA, Lin PL, Scanga CA, and Flynn JL. 2017 Rhesus macaques are more susceptible to progressive tuberculosis than cynomolgus macaques: A quantitative comparison. *Infection and immunity*: IAI. 00505–00517.
62. Ray JCJ, Flynn JL, and Kirschner DE. 2009 Synergy between individual TNF-dependent functions determines granuloma performance for controlling Mycobacterium tuberculosis infection. The Journal of Immunology 182: 3706–3717. [PubMed: 19265149]
63. Marino S, El-Kebir M, and Kirschner D. 2011 A hybrid multi-compartment model of granuloma formation and T cell priming in tuberculosis. Journal of theoretical biology 280: 50–62. [PubMed: 21443879]
64. Segovia-Juarez JL, Ganguli S, and Kirschner D. 2004 Identifying control mechanisms of granuloma formation during M. tuberculosis infection using an agent-based model. Journal of theoretical biology 231: 357–376. [PubMed: 15501468]
65. Warsinske HC, DiFazio RM, Linderman JJ, Flynn JL, and Kirschner DE. 2017 Identifying mechanisms driving formation of granuloma-associated fibrosis during Mycobacterium tuberculosis infection. Journal of theoretical biology 429: 1–17. [PubMed: 28642013]
66. Marino S, Hogue IB, Ray CJ, and Kirschner DE. 2008 A methodology for performing global uncertainty and sensitivity analysis in systems biology. Journal of theoretical biology 254: 178–196. [PubMed: 18572196]
67. Renardy M, Evans S, Hult C, Linderman JJ, Kirschner D 2019 Global sensitivity analysis of biological multi-scale models. Current Opinion in Biomedical Engineering.
68. Alden K, Read M, Timmis J, Andrews PS, Veiga-Fernandes H, and Coles M. 2013 Spartan: a comprehensive tool for understanding uncertainty in simulations of biological systems. PLoS computational biology 9: e1002916. [PubMed: 23468606]
69. Team, R. C. 2018 R: A language and environment for statistical computing. R Foundation for Statistical Computing, Vienna, Austria.
70. Schlaak J, Schmitt E, Hüls C, zum Büschenfelde K-HM, and Fleischer B. 1994 A sensitive and specific bioassay for the detection of human interleukin-10. Journal of immunological methods 168: 49–54. [PubMed: 8288894]
71. Keubler LM, Buettner M, Häger C, and Bleich A. 2015 A Multihit Model: Colitis Lessons from the Interleukin-10–deficient Mouse. Inflammatory bowel diseases 21: 1967. [PubMed: 26164667]
72. Correa I, Veny M, Esteller M, Piqué JM, Yagüe J, Panés J, and Salas A. 2009 Defective IL-10 production in severe phenotypes of Crohn's disease. Journal of leukocyte biology 85: 896–903. [PubMed: 19237638]
73. Ouyang W, Rutz S, Crellin NK, Valdez PA, and Hymowitz SG. 2011 Regulation and functions of the IL-10 family of cytokines in inflammation and disease. Annual review of immunology 29: 71–109.

74. Love C, Tomas MB, Tronco GG, and Palestro CJ. 2005 FDG PET of infection and inflammation. Radiographics : a review publication of the Radiological Society of North America, Inc 25: 1357–1368.
75. Ganchua SKC, Cadena AM, Maiello P, Gideon HP, Myers AJ, Junecko BF, Klein EC, Lin PL, Mattila JT, and Flynn JL. 2018 Lymph nodes are sites of prolonged bacterial persistence during Mycobacterium tuberculosis infection in macaques. PLoS pathogens 14: e1007337–e1007337. [PubMed: 30383808]
76. Borthwick LA, Wynn TA, and Fisher AJ. 2013 Cytokine mediated tissue fibrosis. Biochimica et biophysica acta (BBA)-molecular basis of disease 1832: 1049–1060. [PubMed: 23046809]
77. Laboratory, U. C. T. GranSim. University of Michigan.
78. Warsinske HC, Pienaar E, Linderman JJ, Mattila JT, and Kirschner DE. 2017 Deletion of TGF-beta1 Increases Bacterial Clearance by Cytotoxic T Cells in a Tuberculosis Granuloma Model. Front Immunol 8: 1843. [PubMed: 29326718]
79. Ejrnaes M, Filippi CM, Martinic MM, Ling EM, Togher LM, Crotty S, and von Herrath MG. 2006 Resolution of a chronic viral infection after interleukin-10 receptor blockade. The Journal of Experimental Medicine 203: 2461–2472. [PubMed: 17030951]
80. Tian Y, Mollo SB, Harrington LE, and Zajac AJ. 2016 IL-10 Regulates Memory T Cell Development and the Balance between Th1 and Follicular Th Cell Responses during an Acute Viral Infection. The Journal of Immunology 197: 1308–1321. [PubMed: 27402701]
81. Biswas PS, Pedicord V, Ploss A, Menet E, Leiner I, and Pamer EG. 2007 Pathogen-specific CD8 T cell responses are directly inhibited by IL-10. Journal of immunology (Baltimore, Md. : 1950) 179: 4520–4528.
82. Brockman MA, Kwon DS, Tighe DP, Pavlik DF, Rosato PC, Sela J, Porichis F, Le Gall S, Waring MT, Moss K, Jessen H, Pereyra F, Kavanagh DG, Walker BD, and Kaufmann DE. 2009 IL-10 is up-regulated in multiple cell types during viremic HIV infection and reversibly inhibits virus-specific T cells. Blood 114: 346–356. [PubMed: 19365081]
83. Wangoo A, Laban C, Cook HT, Glenville B, and Shaw R. 1997 Interleukin-10-and corticosteroid-induced reduction in type I procollagen in a human ex vivo scar culture. International journal of experimental pathology 78: 33–41. [PubMed: 9166103]
84. Shi J-H, Guan H, Shi S, Cai W-X, Bai X-Z, Hu X-L, Fang X-B, Liu J-Q, Tao K, and Zhu X-X. 2013 Protection against TGF-β1-induced fibrosis effects of IL-10 on dermal fibroblasts and its potential therapeutics for the reduction of skin scarring. Archives of dermatological research 305: 341–352. [PubMed: 23321694]
85. Sziksz E, Pap D, Lippai R, Béres NJ, Fekete A, Szabó AJ, and Vannay Á. 2015. Fibrosis related inflammatory mediators: role of the IL-10 cytokine family. Mediators of inflammation 2015.
86. Hoffmann KF, Cheever AW, and Wynn TA. 2000 IL-10 and the dangers of immune polarization: excessive type 1 and type 2 cytokine responses induce distinct forms of lethal immunopathology in murine schistosomiasis. The Journal of Immunology 164: 6406–6416. [PubMed: 10843696]
87. Mi S, Li Z, Yang H-Z, Liu H, Wang J-P, Ma Y-G, Wang X-X, Liu H-Z, Sun W, and Hu Z-W. 2011 Blocking IL-17A promotes the resolution of pulmonary inflammation and fibrosis via TGF-β1–dependent and–independent mechanisms. The Journal of Immunology 187: 3003–3014. [PubMed: 21841134]
88. Borthwick L 2016 The IL-1 cytokine family and its role in inflammation and fibrosis in the lung In Seminars in immunopathology. Springer 517–534.
89. Gasse P, Riteau N, Vacher R, Michel M-L, Fautrel A, Di Padova F, Fick L, Charron S, Lagente V, and Eberl G. 2011 IL-1 and IL-23 mediate early IL-17A production in pulmonary inflammation leading to late fibrosis. PloS one 6: e23185. [PubMed: 21858022]
90. Fielding CA, Jones GW, McLoughlin RM, McLeod L, Hammond VJ, Uceda J, Williams AS, Lambie M, Foster TL, and Liao C-T. 2014 Interleukin-6 signaling drives fibrosis in unresolved inflammation. Immunity 40: 40–50. [PubMed: 24412616]
91. Azuma A, Li YJ, Abe S, Usuki J, Matsuda K, Henmi S, Miyauchi Y, Ueda K, Izawa A, and Sone S. 2005 Interferon-β inhibits bleomycin-induced lung fibrosis by decreasing transforming growth factor-β and thrombospondin. American journal of respiratory cell and molecular biology 32: 93–98. [PubMed: 15557019]

92. Lin PL, Dartois V, Johnston PJ, Janssen C, Via L, Goodwin MB, Klein E, Barry CE, and Flynn JL. 2012 Metronidazole prevents reactivation of latent Mycobacterium tuberculosis infection in macaques. Proceedings of the National Academy of Sciences 109: 14188–14193.

93. DiFazio RM, Mattila JT, Klein EC, Cirrincione LR, Howard M, Wong EA, and Flynn JL. 2016 Active transforming growth factor-β is associated with phenotypic changes in granulomas after drug treatment in pulmonary tuberculosis. Fibrogenesis & tissue repair 9: 6. [PubMed: 27148404]

94. Cyktor JC, Carruthers B, Beamer GL, and Turner J. 2013 Clonal expansions of CD8+ T cells with IL-10 secreting capacity occur during chronic Mycobacterium tuberculosis infection. PloS one 8: e58612. [PubMed: 23472214]

95. Dahl KE, Shiratsuchi H, Hamilton BD, Ellner JJ, and Toossi Z. 1996 Selective induction of transforming growth factor beta in human monocytes by lipoarabinomannan of Mycobacterium tuberculosis. Infection and immunity 64: 399–405. [PubMed: 8550183]

96. Nandi B, and Behar SM. 2011 Regulation of neutrophils by interferon-γ limits lung inflammation during tuberculosis infection. Journal of Experimental Medicine: jem. 20110919.

97. Cicchese JM, Evans S, Hult C, Joslyn LR, Wessler T, Millar JA, Marino S, Cilfone NA, Mattila JT, and Linderman JJ. 2018 Dynamic balance of pro-and anti-inflammatory signals controls disease and limits pathology. Immunological reviews 285: 147–167. [PubMed: 30129209]

Key Points:

- IL-10 is not detrimental to early M. tuberculosis infection outcome.
- Lack of IL-10 influences immune responses and fibrosis in granulomas.
- Modeling predicts that prolonged lack of IL-10 leads to improved infection outcomes.

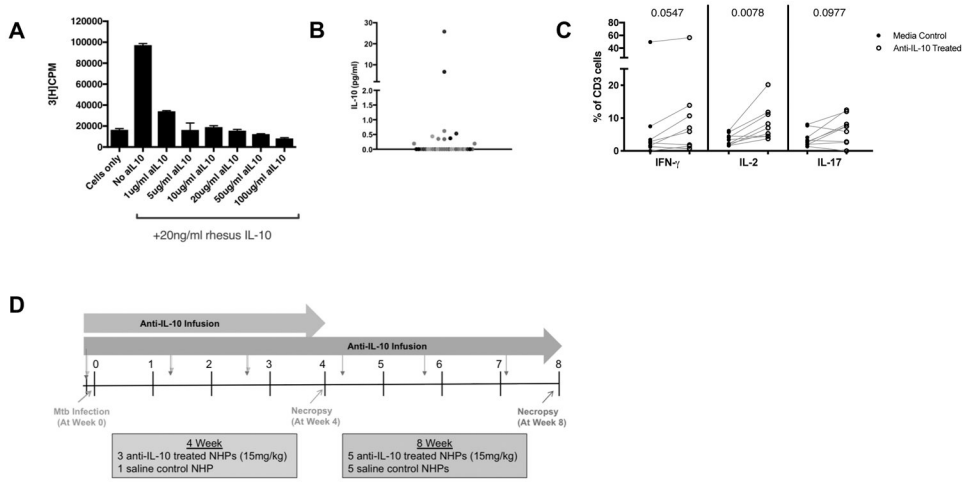

Figure 1. Anti-IL-10 antibody neutralizes macaque IL-10

A) D36 mouse mast cells are IL-10 dependent for cell proliferation. Mast cells with 20ng/ml rhesus IL-10 proliferate, while mast cells with rhesus IL-10 neutralized by varying concentrations of macaque anti-IL-10 antibody have reduced proliferation, as measured by tritiated-thymidine uptake levels. Bars represent means of duplicates, error bars represent standard deviations. B) There is a wide range of IL-10 concentrations in lung granulomas and clusters from Mtb-infected NHPs (n=12) with infection times 4-52 weeks. Each point is a granuloma, each different shade of gray represents a NHP. C) Excised granulomas with detectable levels of IL-10 (>0.19 pg/ml) were treated with anti-IL-10 antibody (10ug/ml) ex vivo and compared to their untreated media controls for frequencies of cytokine response by flow cytometry. Wilcoxon matched-pairs signed rank test p-values reported. D) Experimental setup for study of IL-10 neutralization in vivo in cynomolgus macaquesAnti-IL-10 antibody infusions began one day before Mtb infection and continued throughout the course of infection, for every 10 days (+/−3 days).

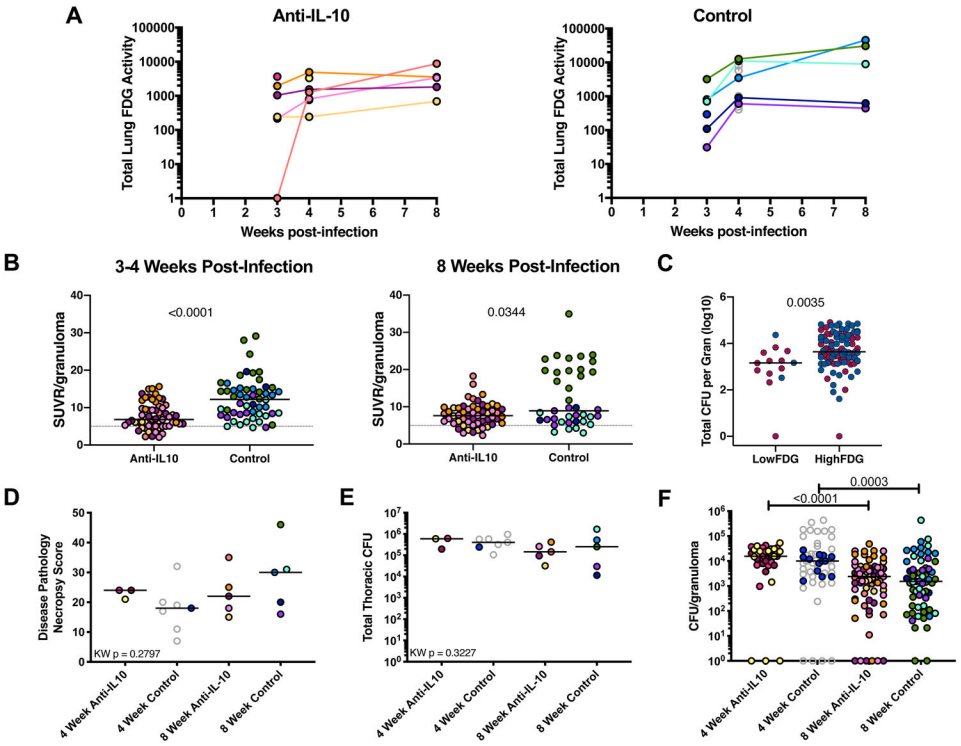

Figure 2. Inflammation in individual granulomas of anti-IL-10 treated NHPs is lower early in Mtb infection, but IL-10 neutralization does not affect overall disease outcome.

A) Total lung inflammation (total ^{18}F-FDG activity) during the course of infection for anti-IL-10 treated and untreated controls. Each color is a NHP. Gray points indicate historical controls. B) ^{18}F-FDG avidity (SUVR) in individual lung granulomas from the 8 week infection NHP cohort, excluding 20516 (medium blue symbol in A and at 4 weeks in B) due to tuberculous disease related lung collapse. Each point is a granuloma, each color is a NHP. Lines at medians. C) In the 8 week infection cohort, individual granulomas were categorized as LowFDG (SUVR < 5) or HighFDG (SUVR ≥ 5) at 3-4 weeks p.i. (see 2B) and bacterial burden was quantified from these individual lung granulomas at 8 weeks post-infection. Lines at medians. Red dots represent granulomas from anti-IL-10 treated animals and blue dots represent granulomas from control animals. D) Gross pathology at necropsy (necropsy score). Each point indicates a NHP, lines at medians. E) Total thoracic CFU quantified at necropsy. Each point indicates a NHP, lines at medians. F) CFU per granuloma at 4 and 8 weeks post-infection. Each point indicates a granuloma, colors indicate NHPs, lines at medians. For B and C, Mann-Whitney test p-values reported. For D, E, and F, Kruskal-Wallis Test was performed and either Kruskal-Wallis p-value (if not statistically significant) or Dunn's Multiple Comparisons adjusted p-values were reported.

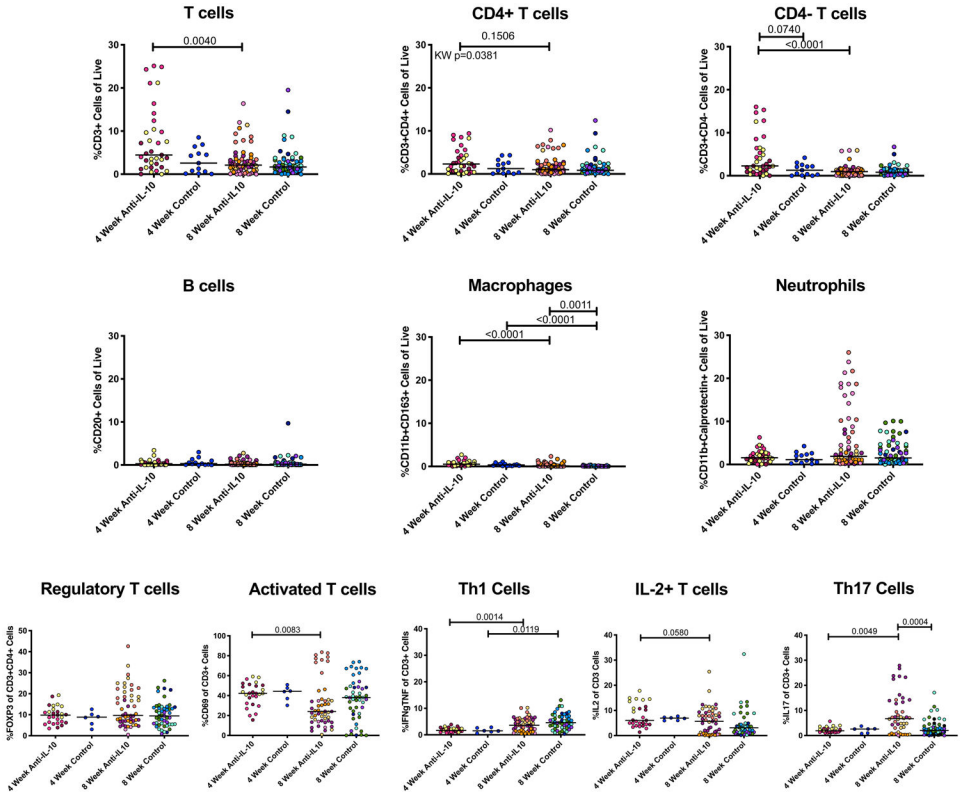

Figure 3. T cell populations and cytokine response in granulomas are similar between anti-IL-10 treated and untreated animals at early time points after Mtb infection.

Cells from excised granulomas were analyzed by intracellular cytokine staining and flow cytometry to identify different cell markers and functionality frequencies in individual granulomas. Each point represents a lung granuloma or cluster, each color is a NHP, lines are at medians. Kruskal-Wallis Test was performed and either Kruskal-Wallis p-value (if not statistically significant) or Dunn's Multiple Comparisons adjusted p-values were reported.

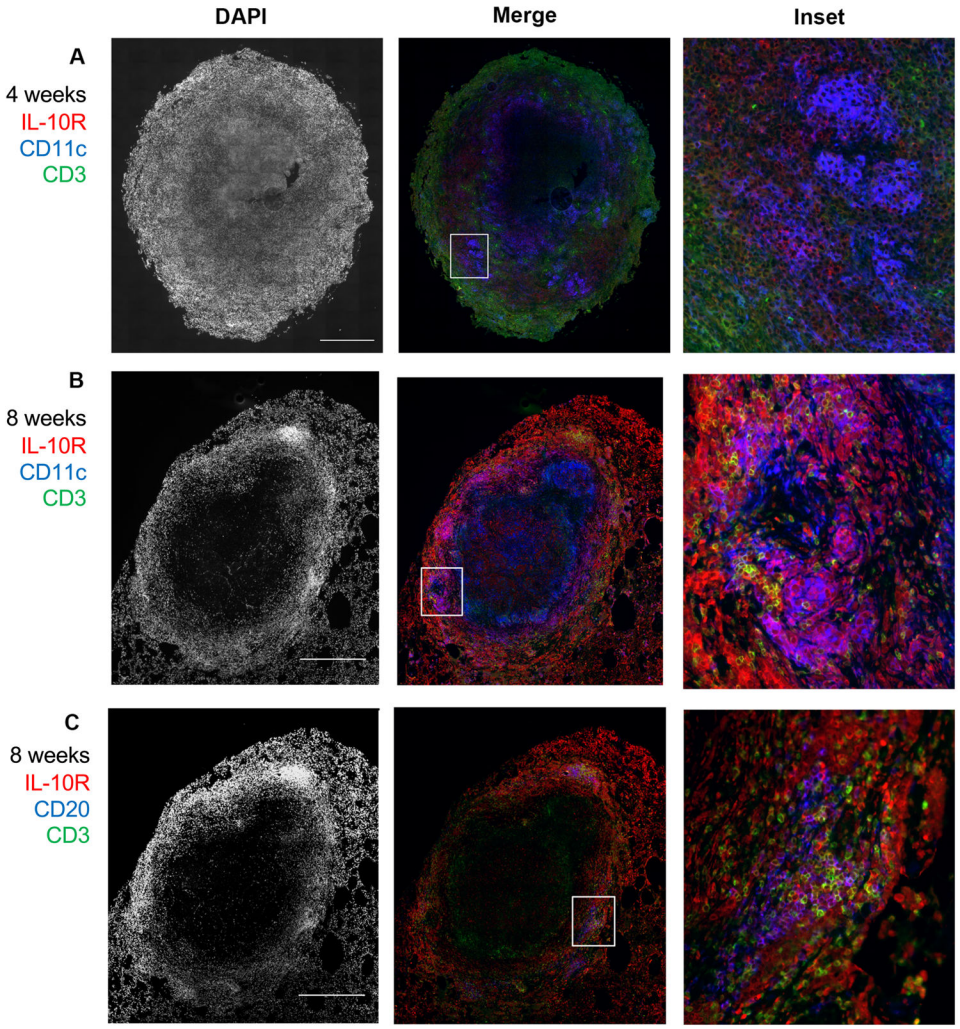

Figure 4. IL-10R co-localizes with non-T cells in TB granulomas.

A representative granuloma from 4 weeks A) or 8 weeks (B) post Mtb infection has more co-localization of IL-10R (red) with CD11c-expressing cells (blue) than CD3-expressing cells (green). (C) The same granuloma as in (B) shows that the CD20 B cells (blue) are IL10R-positive (red), along with a few CD3 cells (green) also expressing IL-10R. Scale bar in DAPI indicates 500um.

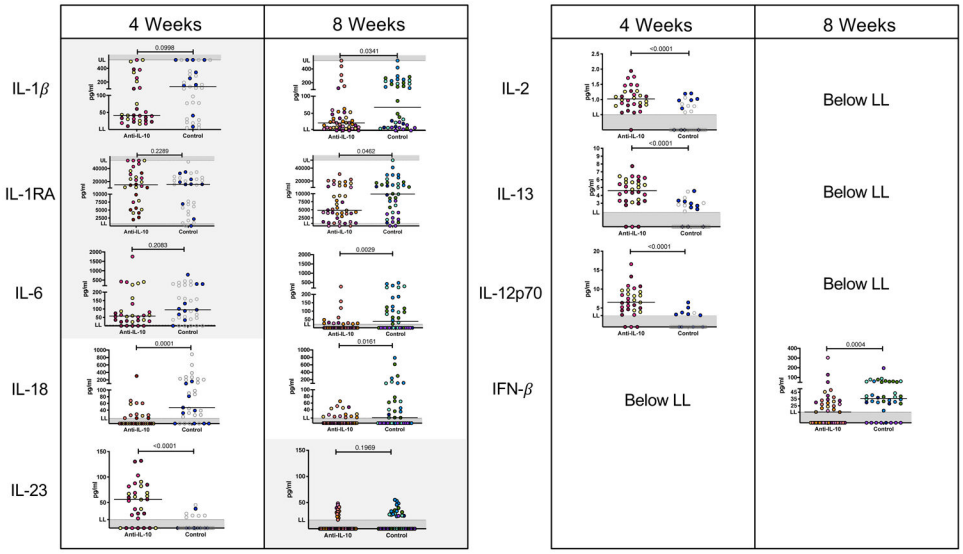

Figure 5. Total cytokine response in lung granulomas are higher in anti-IL-10 treated animals at 4 weeks, but lower at 8 weeks.

Total cytokine concentrations were measured from supernatants from granuloma homogenates by multiplex cytokine assays. Each point represents a granuloma, each color is a NHP. LL= lower limit of quantification, UL = upper limit of quantification. Mann-Whitney test p-values reported and shaded boxes indicate $p > 0.05$.

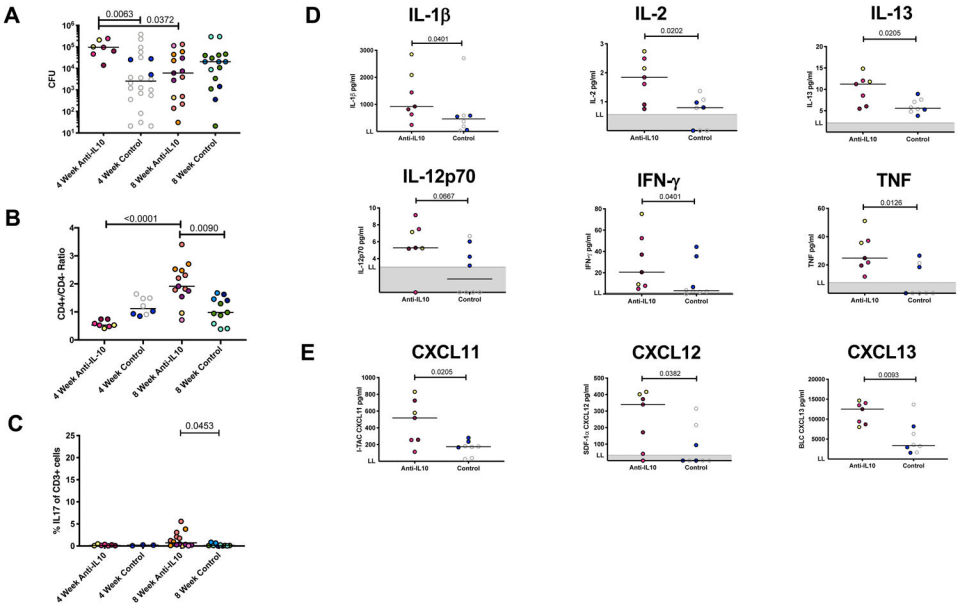

Figure 6. IL-10 inhibits early bacterial burdens, cell recruitment, and immune response in lymph nodes.

A) Bacterial burden is higher in Mtb-infected LNs from anti-IL-10 animals at 4 weeks post-infection. Each point represents a Mtb-infected LN, each color is a NHP (gray indicates historical control). Lines at medians. B) At 4 and 8 weeks post-infection, Mtb-infected LNs of anti-IL-10 treated animals have skewed CD4+/CD4− ratios compared to control animals. Each point represents a Mtb-infected LN, each color is a NHP (gray indicates historical control). Lines at medians. C) Mtb-infected LNs from anti-IL-10 NHPs have higher frequencies of Th17 cells compared to controls at 8 weeks post-infection. Each point represents a Mtb-infected LN, each color is a NHP. Lines at medians. D, E) Total cytokine or chemokine concentrations were measured from supernatants from Mtb-infected LNs by multiplex cytokine assays. LNs of anti-IL-10 treated animals at 4 weeks post-infection had higher cytokine (D) and chemokine (E) levels as compared to controls. Each point represents a Mtb-infected LN, each color is a NHP (gray indicates historical control). LL = lower limit of quantification. For A, B, and C, Kruskal-Wallis Test was performed and Dunn's Multiple Comparisons adjusted p-values were reported. D and E, p-values determined by Mann-Whitney test.

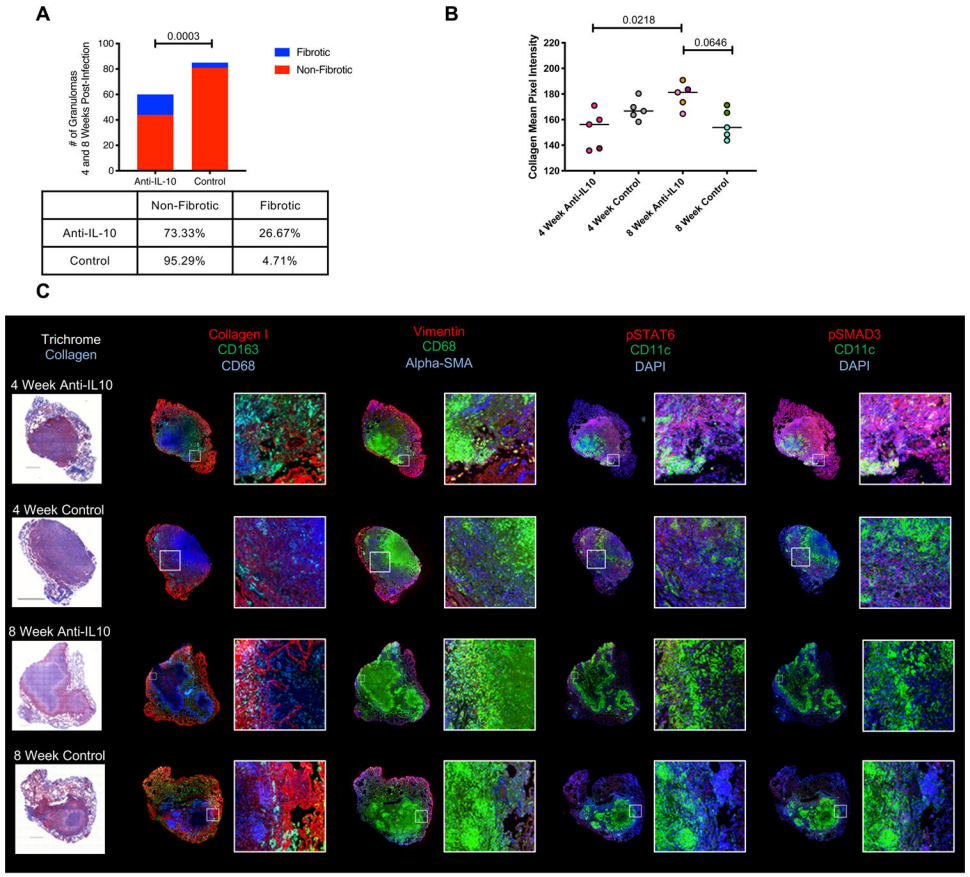

	Non-Fibrotic	Fibrotic
Anti-IL-10	73.33%	26.67%
Control	95.29%	4.71%

Figure 7. IL-10 neutralization leads to increased collagenization and fibrosis in lung granulomas.

A) Anti-IL-10 treated animals have more fibrosis in lung granulomas compared to control animals at the time of necropsy (both 4 and 8 weeks of infection), using a semi-quantitative assessment by a pathologist (EK). Fisher's exact test p-value was reported. B) Lung granulomas from anti-IL-10 treated animals have more collagen at 8 weeks post- Mtb infection than control animals at the time of necropsy, as quantified by mean pixel intensity of blue from Masson's trichrome staining of a random subset of granulomas. Each point represents a granuloma, each color is a NHP (gray indicates historical control). Lines at medians. Kruskal-Wallis Test was performed and Dunn's Multiple Comparisons adjusted p-values were reported. C) Representative granulomas from each treatment group at each time post-infection (4 and 8 weeks) were stained for collagen by Masson's trichrome staining, fibroblast (vimentin), macrophage (CD68), myofibroblast (α-SMA) markers, collagen and macrophage (CD163, CD68) markers, IL-4/IL-13 signaling (pSTAT6) and myeloid (CD11c) markers, and TGF-β signaling (pSMAD3) and myeloid (CD11c) markers as labeled in the figure. White boxes show inset of the area boxed in the granuloma for more detail of representative area with collagen, scale bars in trichrome images represent 500μm.

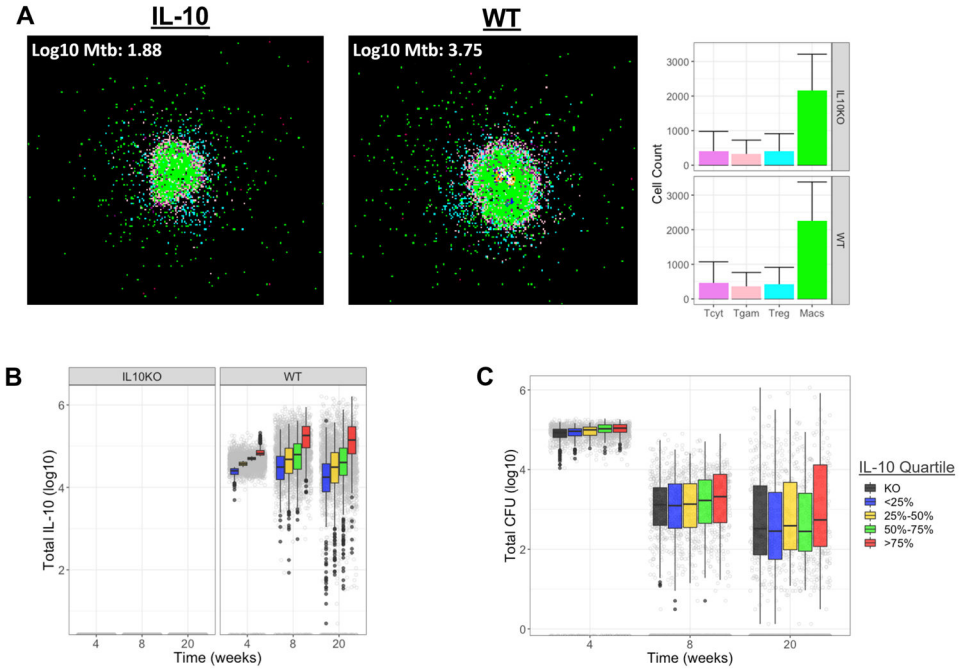

Figure 8. Simulated granulomas recapitulate range of granulomas found *in vivo*.

A) Representative 20 week snapshots of *GranSim*-simulated granulomas under WT and IL-10 KO conditions with average cell counts in each treatment group. Images are taken from a simulation of a 2mm × 2mm piece of lung tissue. Simulated cells colored to show the type of cell they are representing: resting macrophages are green, activated macrophages are blue, infected macrophages are orange, chronically infected macrophages are red, IFN-γ producing T cells are pink, cytotoxic T cells are violet, regulatory T cells are cyan. Caseum is represented as brown compartments and areas of high Mtb burden are shown in white. Bars are colored to correspond to cell types and show mean (solid bar) and standard deviation (error bar) of cell types in all granulomas from each treatment group at 20 weeks post-infection. Range of simulated IL-10 concentrations (B), and CFU profiles (C) in the 636 simulated granulomas at 4, 8, and 20 weeks post-infection in virtual granulomas. Actual amount (gray circles) and distributions within each quantile (boxplots). Error lines demonstrate range of data up to 1.5x the interquartile range, outliers are indicated by black circles.

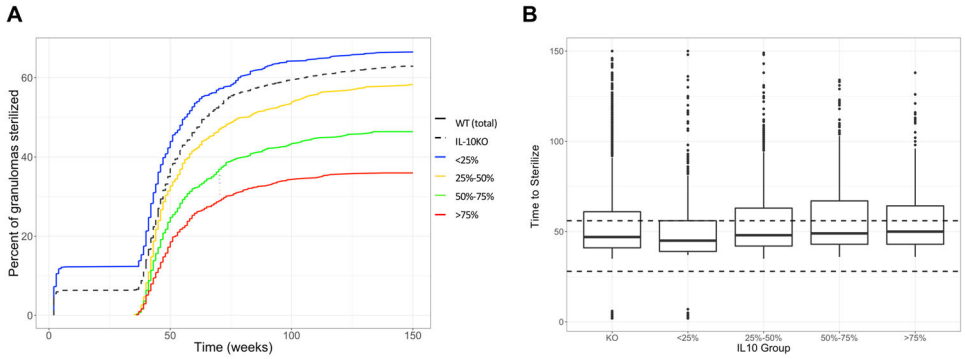

Figure 9. IL-10 depletion increases proportion of sterile granulomas but not time to sterilization.

(A) Sterilization frequencies in granulomas over time at varying levels of IL-10. (B) Time to sterilization for the sterile granulomas within each of the quartiles. Dashed line highlights the 4 week time point used for grouping by quartile. Simulated granulomas with zero CFU were considered to be sterile and the time at which sterilization occurs was recorded (in weeks). Granulomas were grouped by the quantiles of IL-10 in the environment at 4 weeks post infection. Error lines demonstrate range of data up to 1.5x the interquartile range, outliers are indicated by black circles.